

The CCAAT-binding complex mediates azole susceptibility of *Aspergillus fumigatus* by suppressing SrbA expression and cleavage

Chi Zhang, Lu Gao, Yiran Ren, Huiyu Gu, Yuanwei Zhang*, Ling Lu*

Jiangsu Key Laboratory for Microbes and Functional Genomics, Jiangsu Engineering and Technology Research Center for Microbiology; College of Life Sciences, Nanjing Normal University, Nanjing, 210023, China.

*Address correspondence to Yuanwei Zhang, ywzhang@njnu.edu.cn; Ling Lu, linglu@njnu.edu.cn

Abstract

In fungal pathogens, the transcription factor SrbA (a sterol regulatory element-binding protein, SREBP) and CBC (CCAAT binding complex) have been reported to regulate azole resistance by competitively binding the TR34 region (34 *mer*) in the promoter of the drug target gene, *erg11A*. However, current knowledge about how the SrbA and CBC coordinately mediate *erg11A* expression remains limited. In this study, we uncovered a novel relationship between HapB (a subunit of CBC) and SrbA in which deletion of *hapB* significantly prolongs the nuclear retention of SrbA by increasing its expression and cleavage under azole treatment conditions, thereby enhancing Erg11A expression for drug resistance. Furthermore, we verified that loss of HapB significantly induces the expression of the rhomboid protease RbdB, Dsc ubiquitin E3 ligase complex, and signal peptide peptidase SppA, which are required for the cleavage of SrbA, suggesting that HapB acts as a repressor for these genes which contribute to the activation of SrbA by proteolytic cleavage. Together, our study reveals that CBC functions not only to compete with SrbA for binding to *erg11A* promoter region but also to affect SrbA expression, cleavage, and translocation to nuclei for the function, which ultimately regulate Erg11A expression and azole resistance.

Keywords: *Aspergillus fumigatus*; CCAAT-binding complex; SrbA; azole resistance; protein cleavage

Introduction

To date, modern triazole antifungals, such as voriconazole (VRC), itraconazole (ITC) and posaconazole (POC), are still the most common used drugs for *A. fumigatus* infections (Fisher, Hawkins, Sanglard, & Gurr, 2018; Groll et al., 2017; Traunmuller, Popovic, Konz, Smolle-Juttner, & Joukhadar, 2011). However, the emergence of azole-resistant isolates resulting from continued azole stress or natural mutation leads to therapeutic failures and an increase in mortality (Chowdhary, Sharma, & Meis, 2017; Denning & Bromley, 2015; Snelders et al., 2008). Thus, understanding potential azole resistance mechanisms is key for developing new drugs and managing aspergillosis.

Previous studies have provided convincing evidence that azoles work as antifungals by targeting the key ergosterol biosynthesis enzymes lanosterol 14 α -demethylase Erg11 (also known as Cyp51) encoded by two homologous genes, *erg11A* (*cyp51A*) and *erg11B* (*cyp51B*), resulting in an accumulation of 14 α -methyl sterols (Becher & Wirsal, 2012; Georgopapadakou & Walsh, 1996; Joseph-Horne, Hollomon, Manning, & Kelly, 1996). Excess 14 α -methyl sterols impair fungal growth by altering cell membrane permeability and stability (Cowen & Steinbach, 2008; Georgopapadakou & Walsh, 1996; Geria & Scheinfeld, 2008). Recent studies have proposed that azole antifungals also exert their fungicidal activity by triggering the synthesis of cell wall carbohydrate patches that penetrate the plasma membrane, thereby killing the fungus (Geissel et al., 2018). Investigation of azole-resistant *A. fumigatus* suggests that the primary genetic alteration responsible for azole resistance is found within the *erg11A* locus (Burks, Darby, Gomez Londono, Momany, & Brewer, 2021). Among these azole-resistant isolates, the substitution of leucine 98 for histidine (L98H) in the *erg11A* gene along with two copies of a specific 34-bp tandem repeat (TR34) in the *erg11A* promoter (TR34/L98H) resulted in the overexpression of *erg11A*, which was found to be the predominant resistance mechanism (Chowdhary et al., 2017; Mellado et al., 2007; Snelders et al., 2008; J. X. Zhang et al., 2019). Understanding the regulatory mechanisms of *erg11A* expression can provide important insight into azole resistance mechanisms in fungal pathogens.

The expression of *erg11A* has been reported to be regulated by several transcription factors, including SrbA, AtrR, CBC (CCAAT-binding complex), and NCT complex (negative cofactor two A and B), by directly binding to the promoter region of *erg11A* and consequently regulating azole susceptibility (Furukawa, Scheven, et al., 2020; J. X. Zhang et al., 2019). SrbA, a transcriptional regulator that belongs to the sterol regulatory element-binding protein (SREBP) family, directly binds to the 34 *mer* of *erg11A* promoter and positively regulate *erg11A* expression to resist azoles (Bat-Ochir et al., 2016; Blosser & Cramer, 2012; Willger et al., 2012; Willger et al., 2008). SrbA also binds

to its own promoter to autoregulate its expression, as well as the promoters of sterol biosynthesis-related genes in response to hypoxia (Blatzer et al., 2011; Chung et al., 2014). During hypoxia, endoplasmic reticulum (ER)-associated full-length SrbA undergoes protein cleavage involving the rhomboid protease RbdB, Dsc ubiquitin E3 ligase complex (DscA-E), and signal peptide peptidase SppA, resulting in the release of the N-terminal helix-loop-helix (HLH) transcription factor domain into the nucleus to function as a transcription factor (Bat-Ochir et al., 2016; Dhingra et al., 2016; Vaknin et al., 2016; Willger et al., 2012). The nuclear translocation of the N-terminal SrbA also occurs upon azole stress in *A. fumigatus* (Song, Zhai, & Lu, 2017). Consistent with the defective phenotypes observed in the *srbA* deletion mutant under hypoxia and azole conditions, *dscA-E* null mutants show increased susceptibility to hypoxia and azole drugs (Dhingra et al., 2016; Willger et al., 2012). The Zn₂-Cys₆ transcription factor AtrR has also been shown to be a positive regulator of *erg11A* in *A. fumigatus*. Similar to SrbA, the binding site of AtrR also falls in the 34 *mer* region of the *erg11A* promoter (Hagiwara et al., 2017; Paul et al., 2019). CBC, a heterotrimer composed of HapB, HapC, and HapE, is a negative regulatory complex of *erg11A* in *A. fumigatus*. CBC directly binds to the CGAAT motif within the 34 *mer* of the *erg11A* promoter, and CBC dysfunction increases *A. fumigatus* resistance to azoles (Gsaller et al., 2016). Notably, a clinically relevant HapE^{P88L} mutation in *A. fumigatus* is reported to significantly perturb the binding affinity of CBC to the *erg11A* promoter, resulting in an azole-resistant phenotype (Camps et al., 2012; Hortschansky, Haas, Huber, Groll, & Brakhage, 2017). Recently, the subunits of *A. fumigatus* NCT complex (negative cofactor two A and B), NctA and NctB, have been identified as a key regulator of azole resistance by directly binding to the TATA box-like AT-rich motifs within promoter regions of *erg11A*, *hapC*, *srbA* and *atrR* and regulating their expressions (Furukawa, van Rhijn, et al., 2020). Several studies have implicated that the molecular mechanism of azole resistance in *A. fumigatus* is highly complex and tightly regulated by a network of transcriptional activators and repressors. In this study, we analyzed an isolate 415-2 selected from our previously reported azole-resistant *A. fumigatus* library (Wei et al., 2017). Through next-generation sequencing (NGS), we successfully identified a nonsense mutation in *hapB* conferring 415-2 azole resistance. Based on a previous study showing that azole tolerance is governed by the opposing actions of SrbA and CBC on *erg11A* expression, we found that the increased expression of Erg11A and azole resistance induced by loss of HapB is dependent on SrbA. Additionally, we found that the lack of HapB not only increases SrbA expression but also promotes SrbA cleavage and nuclear translocation, which is probably due to the increased expression of RbdB, the Dsc complex, and SppA. These findings broaden our understanding of how SrbA and CBC coordinately regulate Erg11A expression and azole resistance and may provide a

potential avenue for overcoming the resistance to azole drugs.

Experimental procedures

Strains, media, and culture conditions

All *A. fumigatus* strains used in this study are listed in Table A1 (Appendix). In general, these strains were grown on solid minimal media (MM), which contained 0.02 g/ml agar, 0.01 g/ml glucose, 1 ml/L trace elements, and 50 ml/L 20 × salt solution (C. Zhang & Lu, 2017). The liquid MM recipe does not contain agar. Uridine (5 mM) and uracil (10 mM) are required for uracil and uridine auxotrophic strains. To test the sensitivity of *A. fumigatus* to azole drugs, ITC and VRC were supplemented in MM or MM plus uridine and uracil (MMUU). For the plate assay, a 2 µl slurry containing 2×10^4 spores was spotted onto solid MM at 37°C for 2 or 2.5 days. Longer culture time (4 days) was required for the observation of the growth phenotypes on MM with ITC or VRC.

Next-generation sequencing analysis (NGS) sequencing and single-nucleotide polymorphism (SNPs) analysis

The fresh conidial spores of isolate 415-2 were inoculated into liquid MM and shaken for 24 h at 37°C at 200 rpm, and the resulting mycelial pellets were dried and extracted to obtain genome DNA (gDNA). The next-generation sequencing (NGS) experiment was performed at Shanghai OE Biotechnology Co., Ltd., as a commercial service. gDNA of 415-2 was sequenced by using the Illumina HiSeq 2000 platform with 100-bp paired-end reads in a high-output mode. An average depth of each nucleotide was gained. Sequence assembly and mapping were referred to the *A. fumigatus* A1163 genome (http://www.ncbi.nlm.nih.gov/assembly/GCA_000150145.1). Analysis of mapping quality and SNPs was performed by using a next-generation sequencing data analysis suite, SHORE software.

Constructs for deletion, truncation, and GFP labeling strains

Strains (Δ *erg11A*, *hapB*¹⁶⁵, Erg11A-GFP, SppA-GFP, RbdB-GFP, and DscA/B/C/D/E-GFP) were constructed at their native locus by our MMEJ-CRISPR system as described previously (C. Zhang & Lu, 2017; C. Zhang, Meng, Wei, & Lu, 2016). The sgRNA targeting the related gene was synthesized using the MEGAscript T7 Kit (Invitrogen). The corresponding repair templates with microhomology arms were obtained by PCR. Then, the repair template and sgRNA were transformed into a Cas9-expressing *A. fumigatus* strain (ZC03/WT). WT^{GFP-SrbA}, GFP-SrbA^T, SrbA^F, and SrbA^T strains were constructed by transformation with plasmid prg3-AMAI-NotI (Aleksenko & Clutterbuck, 1997; Aleksenko, Gems, & Clutterbuck, 1996). For the recycling usage of the selectable

marker *pyr4*, 1 mg/ml 5-FOA was used to screen recipient strains. For deleting *srbA*, the traditional homologous recombination strategy was employed. All primers are listed in Table A2 (Appendix). *A. fumigatus* transformation was carried out as previously described (C. Zhang & Lu, 2017; C. Zhang et al., 2016).

Molecular cloning

The plasmid p-Ama1-P_{srbA}-gfp-srbA for labeling SrbA with GFP was constructed as follows: using primers Ama1-srbA-F and Ama1-srbA-R, the P_{srbA}-gfp-srbA fragment containing the *srbA* promoter, GFP and *srbA* ORF was amplified from the gDNA of an N-tagged GFP-SrbA strain and then subcloned into the *Bam*HI site of the plasmid prg3-AMAI-NotI, generating the plasmid p-Ama1-P_{srbA}-gfp-srbA.

For colocalization analysis of GFP-SrbA with the nucleus, the plasmid p-Ama1-P_{srbA}-gfp-srbA-P_{gpdA}-rfp-H2A was generated as follows: the fragment P_{srbA}-gfp-srbA was amplified from p-Ama1-P_{srbA}-gfp-srbA with primers Ama1-srbA-F and gpd-srbA-R. The fragment P_{gpdA}-rfp-H2A was amplified from pBARGPE-P_{gpdA}-RFP-H2A using primers gpd-F and Ama1-trpC-R. Then, the two fragments were cloned into the *Bam*HI site of the plasmid prg3-AMAI-NotI, yielding p-Ama1-P_{srbA}-gfp-srbA-P_{gpdA}-rfp-H2A.

To analyze the localization of truncated SrbA (SrbA^T, it contains the residues 1 to 380 of the N-terminus of SrbA), the plasmid p-Ama1-P_{srbA}-gfp-srbA^T-P_{gpdA}-rfp-H2A was generated as follows: The fragment P_{srbA}-gfp-srbA^T was amplified from p-Ama1-P_{srbA}-gfp-srbA with primers Ama1-srbA-F and Ama1-srbA^T-R. The fragment P_{gpdA}-rfp-H2A was amplified from pBARGPE-P_{gpdA}-RFP-H2A using primers gpd-srbA^T-R and Ama1-trpC-R. Then, the two fragments were cloned into the *Bam*HI site of the plasmid prg3-AMAI-NotI, yielding p-Ama1-P_{srbA}-gfp-srbA^T-P_{gpdA}-rfp-H2A.

The plasmid p-Ama1-P_{srbA}-srbA^F/srbA^T was generated as follows: the fragment P_{srbA}-srbA^F/P_{srbA}-srbA^T was amplified from the gDNA of *A. fumigatus* with primers Ama1-srbA-F and Ama1-srbA-R/Ama1-srbA^T-R. Then, the fragment was subcloned into the *Bam*HI site of the plasmid prg3-AMAI-NotI, yielding p-Ama1-P_{srbA}-srbA^F/srbA^T.

The above plasmids were transformed into different background strains, which are listed in data Table A1(Appendix).

Fluorescence microscopy

Fresh spores in 0.5 ml of liquid MM were grown under different treatment conditions (see legends) on sterile glass at 37°C after a set time. The coverslips with hyphae were gently washed with PBS

buffer three times and then fixed with 4% paraformaldehyde. Then, hyphae were washed again with PBS. To detect nuclei, the hyphae were stained with Hoechst 33528 at a final concentration of 0.1 mg/ml for 30 minutes. The fluorescent images of the cells were directly captured with a Zeiss Axio Imager A1 microscope (Zeiss, Jena, Germany).

Quantitative real-time PCR (qRT-PCR) analysis

Fresh *A. fumigatus* conidia were grown in MM in a rotary shaker at 220 rpm at 37°C for 48 h. For measuring the relative mRNA expression levels of target genes, total RNA of related strains was extracted using the UNIQ-10 Column TRIzol Total RNA Isolation Kit (Sangon Biotech, B511361-0020), following the manufacturer's introduction. Then, cDNA synthesis was performed with the HiScript II Q RT SuperMix for qPCR Kit (Vazyme, R223-01). For detecting the relative *srbA* gene copy number, the gDNA of *A. fumigatus* was extracted using Ezup Column Fungi Genomic DNA Purification Kit (Sangon Biotech, B518259-0050). At least three biological replicates had been performed for each independent assay. The relative transcript levels of target genes and *srbA* gene copy number were calculated by the comparative threshold cycle (ΔCT) and normalized against the expression of *tubA* mRNA level and *tubA* gene copy number, respectively. The difference of the relative mRNA expression and *srbA* gene copy number was determined as $2^{-\Delta\Delta\text{CT}}$. All the RT-qPCR or qPCR primers and annotations are listed in data Table A2 (Appendix).

Western blotting

To extract GFP fusion proteins from *A. fumigatus* mycelia, 10^8 conidia were inoculated into 100 ml of liquid MM under different treatment conditions (see legends) for a set time. Mycelia were collected, frozen in liquid nitrogen, and ground with a mortar and pestle. In general, protein extraction was performed using a previously described alkaline lysis strategy (Nandakumar, Shen, Raman, & Marten, 2003). For extracting the nucleoprotein, the commercial nucleoprotein extraction kit (Beyotime, P0027) was used according to the manufacturer's instructions. The GFP fusion protein was detected by using an anti-GFP mouse monoclonal antibody (Roche) at a 1:3,000 dilution. Actin mouse monoclonal antibody (Proteintech, 66009-1) at a 1:5,000 dilution against actin was used as an internal loading control. Detailed procedures of protein extraction and western blotting were described previously (Nandakumar et al., 2003; C. Zhang, Meng, Gu, Ma, & Lu, 2018; C. Zhang et al., 2016).

Recombinant CBC protein purification and electrophoretic mobility shift assay (EMSA)

To express His-labeled CBC subunits *in vitro*, the exons of *hapB*, *hapC*, and *hapE* were amplified with three pairs of primers EmsA-hapB-F/EmsA-hapB-R, EmsA-hapC-F/EmsA-hapC-R, and EmsA-hapE-F/EmsA-hapE-R, respectively, and then ligated into the pET30a vector, subsequently transformed into BL21(DE3) Competent Cells were grown in LB medium at 37°C to an OD600 between 0.6 and 0.8, followed by addition of 0.1 mM isopropyl β -D-thiogalactoside. Protein purification was performed as previously described using a rapid Ni-nitrilotriacetic acid (NTA) agarose minicolumn (Huang, Shang, Chen, Gao, & Wang, 2015). EMSA was carried out according to previously described with minor modifications (Huang et al., 2015; Long et al., 2018). In briefly, each reaction contains consisted of 6 μ l of 5 \times EMSA binding buffer, 1.5 μ l of 1 mg/ml salmon sperm DNA (nonspecific competitor), 60 ng Cy5-labeled probe (double-stranded DNA), 0.5 μ g HapB, 0.8 μ g HapC, and 0.6 μ g HapE. For competitive testing, a 30-fold nonlabeled DNA probe (1.8 μ g) as a competitive cold probe was added to the reaction. To confirm the specific binding of CBC to the binding motif CCAAT, the CCAAT motif within the promoter of the target gene was randomly mutated into a non-CCAAT sequence. The reaction mixtures were incubated at 37°C for 0.5 hours and then separated on a 5% polyacrylamide gel in 0.5 \times Tris-borate EDTA buffer. Subsequently, the Cy5-labeled probes were detected with an Odyssey machine (LI-COR).

Results

The azole resistance of isolate 415-2 is due to the *hapB* mutation

Our previous study has obtained a library of azole-resistant strains through a long-term induction of azole treatment, however, the resistance mechanisms for a majority of these isolates have not been experimentally investigated (Wei et al., 2017). From this library, we found isolate 415-2 without the mutations in *erg11A* showed high resistance to azoles. In comparison to the wild-type strain, isolate 415-2 displayed partial growth defects and high resistance to ITC and VRC (Figure 1a). To identify the potential mutated genes leading to azole resistance, next-generation sequencing (NGS) was implemented on isolate 415-2. After BLAST analysis of the whole genomic sequence assembly based on the *A. fumigatus* A1163 genome, hundreds of single nucleotide polymorphisms (SNPs) were detected in the 415-2 genome (Figure 1b). Most of these SNPs were located in untranslated regions (UTRs), and 38 SNPs existed within the open reading frame (ORF), which contained 23 missense mutations, 2 nonsense mutations, 11 silent mutations, and 2 mutations in splice regions. Notably, one of the two nonsense mutations created a premature stop codon with the *hapB* gene at amino acid position 165 that led to the premature transcription termination of *hapB*. HapB is a

subunit of CBC, which is a multimeric transcription factor complex comprising three subunits (HapB/HapC/HapE) and can bind to CC(G)AAT motif (Gsaller et al., 2016). Inactivation of the CBC by the absence of any of its subunits increases tolerance to different classes of drugs targeting ergosterol biosynthesis, including azoles, allylamines (terbinafine), and statins (simvastatin) (Gsaller et al., 2016). To test whether the azole resistance of isolate 415-2 results from dysfunction of HapB/CBC, we transformed a wild-type *hapB* gene into isolate 415-2, generating 415-2^{hapB} strain. As shown in Figure 1a, 415-2^{hapB} exhibited similar colony growth and azole susceptibility to the wild-type strain, demonstrating that the loss of HapB contributes to the azole resistance of 415-2 isolate. Moreover, *hapB* truncation mutant that mimics the mutation in 415-2 isolate (*hapB*¹⁶⁵) and the CBC deletion mutant ($\Delta hapB$, $\Delta hapC$, and $\Delta hapE$) phenocopied the 415-2 mutant with or without treatment of azole (Figure 1a), further demonstrating that the azole resistance of isolate 415-2 is due to dysfunction of the HapB/CBC complex.

Increased expression of Erg11A and azole resistance induced by loss of HapB is dependent on SrbA

A previous study showed that CBC represses the mRNA expression of *erg11A* by binding the azole resistance-associated 34 *mer* in the *erg11A* promoter (Gsaller et al., 2016). To further explore whether CBC and SrbA coordinately control Erg11A expression at the protein level, we labeled GFP at the C-terminus of Erg11A in the wild-type, $\Delta hapB$, $\Delta srbA$, and $\Delta hapB\Delta srbA$ background strains. Immunoblotting analysis and fluorescence microscopic observation were performed to determine Erg11A-GFP fusion protein expression in related strains in the presence or absence of ITC. Consistent with the increase in *erg11A* mRNA expression after treatment with azole drugs ITC and VRC (Blosser & Cramer, 2012; Du et al., 2021), the protein expression of Erg11A-GFP also displayed a significant elevation after exposure to ITC for 2 h (Figure 2a). Especially, enhanced Erg11A-GFP protein expression was much greater in $\Delta hapB$ than that in wild-type under the ITC treatment condition. Interestingly, the protein expression of Erg11A-GFP was almost completely suppressed in $\Delta srbA$ and $\Delta hapB\Delta srbA$ compared to that of wild-type strain irrespective of ITC treatment, confirming that SrbA is required for Erg11A protein expression. In line with immunoblotting results, fluorescence observation also showed that Erg11A-GFP exhibited stronger GFP signals with the endoplasmic reticulum (ER)-localized pattern in the $\Delta hapB$ strain than that in the wild-type strain, and the GFP signals were barely observed in the $\Delta srbA$ and $\Delta hapB\Delta srbA$ strains (Figure 2b). Moreover, the phenotypic analysis showed that $\Delta hapB\Delta srbA$ presented a sensitive phenotype on ITC/VRC-amended medium, which is similar to the $\Delta srbA$ strain (Figure 2c),

suggesting that the increased expression of Erg11A and azole resistance induced by loss of HapB is dependent on SrbA.

The protein expression and localization of SrbA and HapB under azole treatment conditions

Previous studies indicated that ER membrane-bound SrbA can be cleaved at its C-terminus and delivered into the nucleus to function as a transcription factor after hypoxia induction (Bat-Ochir et al., 2016; Vaknin et al., 2016; Willger et al., 2012). Azole drug has a similar mechanism of action that triggers nuclear transport of SrbA to the nucleus (Song et al., 2017; Vaknin et al., 2016). To explore whether azole-induced SrbA translocation was accompanied by the cleavage of SrbA, we generated the WT^{GFP-SrbA} strain by expressing the GFP-SrbA fusion protein in the wild-type background. The resulting strain exhibited similar growth phenotypes compared to the wild-type strain under conditions with or without ITC treatment (Appendix Figure A1), indicating that the N terminal GFP tag did not affect the function of SrbA. GFP signals were detected in the peripheral areas of the nucleus in WT^{GFP-SrbA} strain without ITC treatment, as indicated by the nuclear dye Hoechst (Figure 3a), indicating its localization in the ER. After ITC treatment for 2 h, GFP-SrbA signals overlapped with the Hoechst signals, indicating the nuclear localization of SrbA. We confirmed that treatment with the DMSO control did not change the ER localization of GFP-SrbA. To determine if SrbA cleavage was associated with its nuclear localization, total protein was extracted from the WT^{GFP-SrbA} strain using alkaline lysis followed by immunoblotting using a GFP antibody. Immunoblotting showed specific bands at approximately 150 kDa with or without ITC treatment, corresponding to the full-length SrbA-GFP fusion protein (hereafter named GFP-SrbA-F; GFP: ~27 kDa, SrbA: ~120 kDa), however, no cleaved SrbA bands were observed (Figure 3b). In contrast, the nuclear forms of SrbA (the cleaved N-terminus, hereafter named GFP-SrbA-N) were clearly visible by using a specific nucleoprotein extraction kit (Figure 3b), suggesting that ITC induces SrbA protein cleavage and nuclear translocation. To explore the effects of ITC on HapB protein, the HapB was labeled with an N-terminus GFP tag at its native locus. The GFP-HapB fusion protein did not cause any morphological phenotypes compared to the parental strain (Appendix Figure A1), indicating that it is fully functional. As shown in Figure 3c, the GFP-HapB fusion protein was constantly located in the nucleus, irrespective of ITC treatment, indicating that the localization of HapB was not affected by ITC. Notably, the immunoblotting analysis showed that ITC treatment could induce upregulation of GFP-HapB expression (Figure 3d), suggesting that the nuclear-localized HapB could respond to azole treatment.

The nuclear form of *SrbA* confers azole resistance and increases the expression of *Erg11A* in *A. fumigatus*

Considering that ITC induces the *SrbA* cleavage and nuclear translocation, we wondered whether the nuclear form of *SrbA* was associated with azole resistance. To test this, we constructed a truncated *SrbA* strain (GFP-*SrbA*^T) that expresses a putative nuclear form of *SrbA* (*SrbA*^T, which contains the first 380 aa of *SrbA*) fused with GFP at its N-terminus under the control of the *srbA* native promoter in the wild-type background (Figure 4a). To examine whether the GFP-*SrbA*^T fusion protein localizes to the nucleus, we coexpressed RFP-tagged histone H2A (RFP-H2A) as a nuclear marker. As shown in Figure 4b, GFP signals of full-length GFP-*SrbA* were detected in the peripheral areas of RFP-H2A, whereas GFP-*SrbA*^T was colocalized with RFP-H2A in minimal medium, indicating that the mutant with a nuclear form of *SrbA* was successfully constructed. To exclude the interference of the GFP tag with the function of *SrbA*^T, we generated a *SrbA*^T strain that expresses *SrbA*^T without a GFP tag in the wild-type background using the AMA1 vector. A *SrbA*^F strain expressing the full-length of *srbA* was also constructed similarly as a control. To exclude the possibility that the AMA1 plasmids may introduce different *srbA* gene copies between *SrbA*^F and *SrbA*^T strains, we compared the relative gene copy number of *srbA* by quantitative real-time PCR (qRT-PCR) analysis. The result showed no significant difference in *srbA* copy number between *SrbA*^F and *SrbA*^T strains (Appendix Figure A2a). The colony phenotype of *SrbA*^T strain was indistinguishable from *SrbA*^F strain on minimal medium but displayed increased resistance to ITC (Figure 4c), indicating the contribution of the nuclear form of *SrbA* to azole resistance. To verify whether expression of *Erg11A* could be changed in the *SrbA*^T strain, we expressed *SrbA*^T and *SrbA*^F in the *Erg11A*-GFP labeled strain, respectively. As shown in Figure 4d, *Erg11A*-GFP expression in the *SrbA*^T strain was significantly higher than that in the *SrbA*^F strain in minimal media. Fluorescence microscopy further confirmed that *Erg11A*-GFP in the *SrbA*^T strain exhibited a strong ER-localization signal, whereas in the *SrbA*^F strain, GFP fluorescence was barely observed (Figure 4e), suggesting that nuclear form of *SrbA* contributes to the increased expression of *Erg11A*, and the amount of nuclear form of *SrbA* in *SrbA*^T strain is greater than that in the *SrbA*^F strain. Taken together, these data suggest that the constitutive nucleus-localized N-terminus of *SrbA* renders *A. fumigatus* resistant to azole by upregulating *Erg11A*.

Lack of *HapB* increases *SrbA* expression and prolongs its nuclear retention.

Based on the above findings, *SrbA* positively regulates *Erg11A* expression by its nuclear form, and

overexpression of Erg11A is the main cause for azole resistance of the *hapB* deletion mutant. We next expressed the GFP-SrbA by AMA1 vector in the $\Delta hapB$ and wild-type background to examine whether a lack of HapB would affect the levels of the nuclear form of SrbA. qRT-PCR analysis showed no significant difference in *srbA* copy number between WT^{GFP-SrbA} and $\Delta hapB$ ^{GFP-SrbA} mutants (Appendix Figure A2b). Using fluorescence microscopy, we examined the localization of GFP-SrbA in the $\Delta hapB$ ^{GFP-SrbA} and WT^{GFP-SrbA}. As shown in Figure 5a, GFP-SrbA showed ER-localized patterns in the $\Delta hapB$ and the wild-type strains when grown in minimal medium without ITC treatment and moved into the nucleus after ITC treatment for 2 and 4 h. Notably, with the prolongation of ITC treatment to 6 h, the nucleus-localized fluorescence of GFP-SrbA in the wild-type strain showed the punctate GFP signals throughout the hyphae. In contrast, GFP-SrbA in $\Delta hapB$ hyphae still exhibited a distinct nuclear localization pattern at the same time-point, which suggests that the lack of HapB prolongs the retention time of GFP-SrbA in the nucleus. Using immunoblotting with a GFP antibody, we examined the cleavage levels of SrbA in the $\Delta hapB$ and its parental wild-type strains after ITC or DMSO treatment for 4 h. As shown in Figure 5b, the $\Delta hapB$ ^{GFP-SrbA} strain showed more accumulation of the nuclear forms of SrbA than the control strain WT^{GFP-SrbA}, even under non-induced conditions with DMSO treatment. In addition, we found that the $\Delta hapB$ mutant showed an increased protein level of SrbA compared to the wild-type strain without ITC treatment, suggesting that HapB could be a negative regulator of SrbA. To confirm this, we conducted the qRT-PCR analysis to compare the *srbA* transcription level in the wild-type and $\Delta hapB$ mutant. As shown in Figure 5c, the mRNA level of *srbA* increased in the $\Delta hapB$ mutant. Previous studies have shown that CBC regulates the expression of downstream targets through binding to the 5'-CCAAT-3' within their promoter regions (Gsaller et al., 2016; Hortschansky et al., 2017; Steidl, Hynes, & Brakhage, 2001). Sequence analysis revealed that two CCAAT motifs are located at position 849 and 195 base pairs (-849 and -195) upstream of the *srbA* translation start site. To further investigate whether CBC can directly bind to these two CCAAT motifs, we expressed and purified the HapB/C/E proteins in *E. coli*, respectively, and then mixed them to form CBC complex for electrophoretic mobility shift assays (EMSA). As shown in Figure 5d, the *srbA* probe 1 (position: -849) mixed with CBC displayed a slow shift compared to the free probe without CBC treatment. Excess of unlabeled probe (cold probe) significantly reduced the binding activity of CBC with the Cy5-labeled probe. Moreover, the mutated probe without the CCAAT motif showed a clear decrease in the binding activity of the upper complex. In comparison, *srbA* probe 2 (position: -195) also exhibited weak binding to CBC complex. These data suggested that the binding of CBC to the *srbA* promoter is dependent on the CCAAT motif.

Upregulation of SppA and the Dsc ubiquitin E3 ligase complex induced by the lack of HapB are responsible for proteolytic cleavage of SrbA

It has been reported that the cleavage of SrbA requires the rhomboid protease RbdB, the Dsc ubiquitin E3 ligase complex composed of five subunits (DscA-E), and the signal peptide peptidase SppA, all of which are critical for translocation of SrbA from the ER into the nucleus and then SrbA could be transcriptionally activated (Figure 6a) (Bat-Ochir et al., 2016; Dhingra et al., 2016; Vaknin et al., 2016; Willger et al., 2012). We wondered whether the increase in the nuclear forms of SrbA in $\Delta hapB$ might be related to the expression of RbdB, the Dsc complex, and SppA. We therefore performed the qRT-PCR to detect the mRNA level of these genes. As shown in Figure 6b, except for *dscB*, the expression level of *rbdB*, *sppA*, and *dscA/C/D/E* was increased in the $\Delta hapB$ mutant compared to that of the wild-type. As the sequence analysis showed that the promoter regions of all these upregulated genes contain at least one CBC binding motif CCAAT, we next selected *dscE*, *rbdB*, and *sppA* to perform EMSA analysis to test whether CBC binds to their promoters, the results showed that CBC can bind to the CCAAT motifs of *dscE* (position -1467), *rbdB* (position -600) and *sppA* (position -170) promoter regions with different degrees, but fails to bind other CCAAT regions of *dscE* (positions -728, -862) and *rbdB* (position -300) *in vitro* (Figure 6c and Appendix Figure A3). To further verify whether CBC could affect the protein expression of RbdB, SppA, and DscA/C/D/E, we tagged these proteins with GFP at the C-terminus under the control of their respective promoters in the wild-type and $\Delta hapB$ backgrounds, respectively. The phenotypic analysis confirmed that the tagged proteins are fully functional, as the resulting strains exhibited a similar growth phenotype to their respective parental strains (Appendix Figure A4). In line with the mRNA level, western blotting analysis showed that, except for the undetected DscA and RbdB expressions, DscC/D/E and SppA fusion proteins in the $\Delta hapB$ strain were increased compared to those in the parental wild-type strain (Figure 6d), indicating that CBC represses the expression of SppA and the DscC/D/E at the protein level. Collectively, these results suggest that CBC represses the expression of SppA, RbdB, and the Dsc ubiquitin E3 ligase complex by binding the promoters of the corresponding genes.

Discussion

In fungi, the transcriptional regulator SrbA and the CBC complex have been reported to transcriptionally regulate the expression of the azole target Erg11A and therefore play critical roles in azole resistance and sterol biosynthesis (Gsaller et al., 2016). It has been reported that both SrbA and CBC can bind to the TR34 region of the *erg11A* promoter, and they perform opposing actions

to govern sterol biosynthesis and azole tolerance. The absence of any of the CBC subunits results in increased tolerance of *A. fumigatus* to azoles mainly due to the increased mRNA expression of *erg11A*. In contrast, the increased azole susceptibility in the *srbA* null mutant strain is the result of *erg11A* transcript insufficiency. In this study, we identified that the non-*erg11A* azole resistance isolate 415-2 harbors a mutation in the *hapB* gene that leads to the premature transcription termination of *hapB*. Importantly, we revealed a potential regulatory mechanism by which the CBC negatively regulates *SrbA* expression by directly binding to *srbA* promoter, and represses *SrbA* cleavage by down-regulating the expression of the rhomboid protease *RbdB*, the Dsc ubiquitin E3 ligase complex, and the signal peptide peptidase *SppA*.

In mammals, low sterol activates ER-localized SREBP by triggering its protein cleavage accompanied by its N-terminal translocation to the nucleus (Bat-Ochir et al., 2016; Brown & Goldstein, 1997, 1998, 1999). A similar mechanism exists in SREBP homolog, *SrbA*, in *Aspergillus* species under hypoxic conditions (Willger et al., 2012). We found that azole also induces the cleavage of *A. fumigatus* *SrbA* and its translocation into the nucleus (Figure 3a) (Song et al., 2017). In addition, expression of the putative nuclear forms of *SrbA* in the wild-type strain increased *Erg11A* protein expression and tolerance to azole (Figure 4c-e). These data suggest that azole exerts a similar influence on *SrbA* cleavage and nuclear translocation. The rhomboid protease *RbdB*, Dsc ubiquitin E3 ligase complex in *A. fumigatus*, and signal peptide peptidase *SppA* in *A. nidulans* are required for the cleavage of *SrbA* precursor protein (Bat-Ochir et al., 2016; Dhingra et al., 2016; Willger et al., 2012). We found that the lack of *HapB* increased the nuclear forms of *SrbA* and prolonged the retention time of *SrbA* in the nucleus under azole treatment conditions (Figure 5a and 5b) may arise as a consequence of the upregulation of *RbdB*, *SppA*, and the Dsc complex (Figure 6b, 6d and 7). In addition, the *HapB* also negatively regulated the expression of *SrbA*, and loss of *HapB* increased the content of the total *SrbA* protein, which could also relatively increase nuclear forms of *SrbA* (Figure 5b and 7). According to previous reports, more than 2000 gene promoters are occupied by the CBC, and the high abundance of CBC binding motifs CC(G)AAT are identified in eukaryotic promoters (Furukawa, Scheven, et al., 2020), suggesting that CBC plays a role as a global regulator. Therefore, these data raise a possibility that *HapB* can negatively mediate the expression and cleavage of *SrbA* to regulate azole resistance besides repressing *erg11A* expression. In line with this hypothesis, our EMSA analysis validated that CBC can specifically bind to *srbA*, *dscE*, *rbdB*, and *sppA* *in vitro* via the conserved CCAAT motifs (*srbA*: position -986 and -195, *dscE*: position -1467, *rbdB*: position -600 and *sppA*: position -170). Previous ChIP-seq analysis has also revealed that the CBC-binding peaks were located at position 849 (-849) and 318 (-318)

base pairs upstream of the *srbA* and *dscE* translational start sites, respectively (Furukawa, Scheven, et al., 2020), however, no typical CCAAT or CGAAT motif was observed in these regions. This may be because the ChIP peaks may result from the indirect binding events via intermediary partners, as the previous study showed that the transcription factor HapX forms a complex with CBC and CBC/HapX complex recognizes other DNA motifs than CC(G)AAT such as 5'-RWT-3' and 5'-TKAN-3' motifs (Furukawa, Scheven, et al., 2020). Nevertheless, our qRT-PCR and western blotting experiments further showed that loss of CBC resulted in increased expression of *SrbA* and the majority of its cleavage-related genes. In addition, since azole drugs and CBC deficiency have been reported to change the sterol profile (Gsaller et al., 2016; Shapiro, Robbins, & Cowen, 2011), we therefore cannot rule out the potential role of altered sterol profile in the regulation of *SrbA* expression and nuclear retention, which needs further investigation and analysis.

Conclusion

In this study, our findings have revealed another plausible mechanism by which CBC dysfunction causes the upregulation of *SrbA*, and *RbdB*, *SppA*, and the *Dsc* complex facilitate *SrbA* activity, which ultimately elevates *Erg11A* expression and azole tolerance, and provides new insight into the molecular mechanism underlying the regulation of azole resistance. A working model summarizing the findings of this study is depicted in Figure 7.

Author contributions

Chi Zhang: Conceptualization (Lead), Data curation (Lead), Formal analysis (Lead), Investigation (Equal), Methodology (Equal), Resources (Equal), Software (Equal), Validation (Equal), Writing-original draft (Equal). Lu Gao: Conceptualization (Equal), Data curation (Equal), Formal analysis (Equal), Investigation (Equal), Methodology (Equal), Resources (Equal). Yiran Ren: Conceptualization (Equal), Methodology (Equal). Huiyu Gu: Conceptualization (Equal), Investigation (Equal). Yuanwei Zhang: Formal analysis (Equal), Funding acquisition (Equal), Methodology (Equal), Project administration (Equal), Supervision (Equal), Writing-original draft (Equal), Writing-review & editing (Equal). Ling Lu: Funding acquisition (Equal), Investigation (Equal), Methodology (Equal), Project administration (Equal), Resources (Equal), Supervision (Equal), Writing-review & editing (Lead).

Acknowledgments

This work was financially supported by the National Key R & D Program of China (2019YFA0904900)

and the National Natural Science Foundation of China (31861133014, 31770086), the Priority Academic Program Development (PAPD) of Jiangsu Higher Education Institutions to L.L. National Natural Science Foundation of China (31900404) and Natural Science Foundation of the Jiangsu Higher Education Institutions of China (19KJB180017) to Y.Z.

Conflict of interest

None declared.

Ethics statement

None required

Data Availability Statement

The data that support the findings of this study are available in this published article and its appendices.

References

- Aleksenko, A., & Clutterbuck, A. J. (1997). Autonomous plasmid replication in *Aspergillus nidulans*: AMA1 and MATE elements. *Fungal Genet Biol*, 21(3), 373-387. doi:10.1006/fgbi.1997.0980
- Aleksenko, A., Gems, D., & Clutterbuck, J. (1996). Multiple copies of MATE elements support autonomous plasmid replication in *Aspergillus nidulans*. *Mol Microbiol*, 20(2), 427-434. doi:10.1111/j.1365-2958.1996.tb02629.x
- Bat-Ochir, C., Kwak, J. Y., Koh, S. K., Jeon, M. H., Chung, D., Lee, Y. W., & Chae, S. K. (2016). The signal peptide peptidase SppA is involved in sterol regulatory element-binding protein cleavage and hypoxia adaptation in *Aspergillus nidulans*. *Mol Microbiol*, 100(4), 635-655. doi:10.1111/mmi.13341
- Becher, R., & Wirsal, S. G. (2012). Fungal cytochrome P450 sterol 14 α -demethylase (CYP51) and azole resistance in plant and human pathogens. *Appl Microbiol Biotechnol*, 95(4), 825-840. doi:10.1007/s00253-012-4195-9
- Blatzer, M., Barker, B. M., Willger, S. D., Beckmann, N., Blosser, S. J., Cornish, E. J., . . . Cramer, R. A. (2011). SREBP coordinates iron and ergosterol homeostasis to mediate triazole drug and hypoxia responses in the human fungal pathogen *Aspergillus fumigatus*. *PLoS Genet*, 7(12), e1002374. doi:10.1371/journal.pgen.1002374
- Blosser, S. J., & Cramer, R. A. (2012). SREBP-dependent triazole susceptibility in *Aspergillus fumigatus* is mediated through direct transcriptional regulation of *erg11A* (*cyp51A*). *Antimicrob Agents Chemother*,

56(1), 248-257. doi:10.1128/AAC.05027-11

Brown, M. S., & Goldstein, J. L. (1997). The SREBP pathway: regulation of cholesterol metabolism by proteolysis of a membrane-bound transcription factor. *Cell*, 89(3), 331-340. doi:10.1016/s0092-8674(00)80213-5

Brown, M. S., & Goldstein, J. L. (1998). Sterol regulatory element binding proteins (SREBPs): controllers of lipid synthesis and cellular uptake. *Nutr Rev*, 56(2 Pt 2), S1-3; discussion S54-75. doi:10.1111/j.1753-4887.1998.tb01680.x

Brown, M. S., & Goldstein, J. L. (1999). A proteolytic pathway that controls the cholesterol content of membranes, cells, and blood. *Proc Natl Acad Sci U S A*, 96(20), 11041-11048. doi:10.1073/pnas.96.20.11041

Burks, C., Darby, A., Gomez Londono, L., Momany, M., & Brewer, M. T. (2021). Azole-resistant *Aspergillus fumigatus* in the environment: Identifying key reservoirs and hotspots of antifungal resistance. *PloS Pathog*, 17(7), e1009711. doi:10.1371/journal.ppat.1009711

Camps, S. M. T., Dutilh, B. E., Arendrup, M. C., Rijs, A. J. M. M., Snelders, E., Huynen, M. A., . . . Melchers, W. J. G. (2012). Discovery of a *hapE* Mutation That Causes Azole Resistance in *Aspergillus fumigatus* through Whole Genome Sequencing and Sexual Crossing. *PloS One*, 7(11), e50034. doi:10.1371/journal.pone.0050034

Chowdhary, A., Sharma, C., & Meis, J. F. (2017). Azole-Resistant Aspergillosis: Epidemiology, Molecular Mechanisms, and Treatment. *J Infect Dis*, 216(suppl_3), S436-S444. doi:10.1093/infdis/jix210

Chung, D., Barker, B. M., Carey, C. C., Merriman, B., Werner, E. R., Lechner, B. E., . . . Cramer, R. A. (2014). ChIP-seq and in vivo transcriptome analyses of the *Aspergillus fumigatus* SREBP SrbA reveals a new regulator of the fungal hypoxia response and virulence. *PloS Pathog*, 10(11), e1004487. doi:10.1371/journal.ppat.1004487

Cowen, L. E., & Steinbach, W. J. (2008). Stress, drugs, and evolution: the role of cellular signaling in fungal drug resistance. *Eukaryot Cell*, 7(5), 747-764. doi:10.1128/EC.00041-08

Denning, D. W., & Bromley, M. J. (2015). How to bolster the antifungal pipeline. *Science*, 347(6229), 1414-1416. doi:10.1126/science.aaa6097

Dhingra, S., Kowalski, C. H., Thammahong, A., Beattie, S. R., Bultman, K. M., & Cramer, R. A. (2016). RbdB, a Rhomboid Protease Critical for SREBP Activation and Virulence in *Aspergillus fumigatus*. *mSphere*, 1(2), e00035-00016. doi:10.1128/mSphere.00035-16

Du, W., Zhai, P., Wang, T., Bromley, M. J., Zhang, Y., & Lu, L. (2021). The C2H2 Transcription Factor SitA Contributes to Azole Resistance by Coregulating the Expression of the Drug Target Erg11A and the Drug Efflux Pump Mdr1 in *Aspergillus fumigatus*. *Antimicrob Agents Chemother*, 65(4), e01839-01820. doi:10.1128/AAC.01839-20

Fisher, M. C., Hawkins, N. J., Sanglard, D., & Gurr, S. J. (2018). Worldwide emergence of resistance to antifungal

- drugs challenges human health and food security. *Science*, 360(6390), 739-742. doi:10.1126/science.aap7999
- Furukawa, T., Scheven, M. T., Misslinger, M., Zhao, C., Hoefgen, S., Gsaller, F., . . . Hortschansky, P. (2020). The fungal CCAAT-binding complex and HapX display highly variable but evolutionary conserved synergetic promoter-specific DNA recognition. *Nucleic Acids Res*, 48(7), 3567-3590. doi:10.1093/nar/gkaa109
- Furukawa, T., van Rhijn, N., Fraczek, M., Gsaller, F., Davies, E., Carr, P., . . . Bromley, M. J. (2020). The negative cofactor 2 complex is a key regulator of drug resistance in *Aspergillus fumigatus*. *Nat Commun*, 11(1), 427. doi:10.1038/s41467-019-14191-1
- Geissel, B., Loiko, V., Klugherz, I., Zhu, Z., Wagener, N., Kurzai, O., . . . Wagener, J. (2018). Azole-induced cell wall carbohydrate patches kill *Aspergillus fumigatus*. *Nat Commun*, 9(1), 3098. doi:10.1038/s41467-018-05497-7
- Georgopapadakou, N. H., & Walsh, T. J. (1996). Antifungal agents: chemotherapeutic targets and immunologic strategies. *Antimicrob Agents Chemother*, 40(2), 279-291. doi:10.1128/AAC.40.2.279
- Geria, A. N., & Scheinfeld, N. S. (2008). Pramiconazole, a triazole compound for the treatment of fungal infections. *IDrugs*, 11(9), 661-670.
- Groll, A. H., Townsend, R., Desai, A., Azie, N., Jones, M., Engelhardt, M., . . . Bruggemann, R. J. M. (2017). Drug-drug interactions between triazole antifungal agents used to treat invasive aspergillosis and immunosuppressants metabolized by cytochrome P450 3A4. *Transpl Infect Dis*, 19(5), e12751. doi:10.1111/tid.12751
- Gsaller, F., Hortschansky, P., Furukawa, T., Carr, P. D., Rash, B., Capilla, J., . . . Bromley, M. J. (2016). Sterol Biosynthesis and Azole Tolerance Is Governed by the Opposing Actions of SrbA and the CCAAT Binding Complex. *PLoS Pathog*, 12(7), e1005775. doi:10.1371/journal.ppat.1005775
- Hagiwara, D., Miura, D., Shimizu, K., Paul, S., Ohba, A., Gono, T., . . . Gomi, K. (2017). A Novel Zn²⁺-Cys⁶ Transcription Factor AtrR Plays a Key Role in an Azole Resistance Mechanism of *Aspergillus fumigatus* by Co-regulating *cyp51A* and *cdr1B* Expressions. *PLoS Pathog*, 13(1), e1006096. doi:10.1371/journal.ppat.1006096
- Hortschansky, P., Haas, H., Huber, E. M., Groll, M., & Brakhage, A. A. (2017). The CCAAT-binding complex (CBC) in *Aspergillus* species. *Biochimica Et Biophysica Acta*, 1860(5), 560-570. doi:10.1016/j.bbagr.2016.11.008
- Huang, W., Shang, Y., Chen, P., Gao, Q., & Wang, C. (2015). MrpacC regulates sporulation, insect cuticle penetration and immune evasion in *Metarhizium robertsii*. *Environ Microbiol*, 17(4), 994-1008. doi:10.1111/1462-2920.12451
- Joseph-Horne, T., Hollomon, D., Manning, N., & Kelly, S. L. (1996). Investigation of the Sterol Composition and

- Azole Resistance in Field Isolates of *Septoria tritici*. *Appl Environ Microbiol*, 62(1), 184-190. doi:10.1128/aem.62.1.184-190.1996
- Long, N. B., Orasch, T., Zhang, S. Z., Gao, L., Xu, X. L., Hortschansky, P., . . . Lu, L. (2018). The Zn(2)Cys(6)-type transcription factor LeuB cross-links regulation of leucine biosynthesis and iron acquisition in *Aspergillus fumigatus*. *PLoS Genet*, 14(10), e1007762. doi:10.1371/journal.pgen.1007762
- Mellado, E., Garcia-Effron, G., Alcazar-Fuoli, L., Melchers, W. J., Verweij, P. E., Cuenca-Estrella, M., & Rodriguez-Tudela, J. L. (2007). A new *Aspergillus fumigatus* resistance mechanism conferring in vitro cross-resistance to azole antifungals involves a combination of *cyp51A* alterations. *Antimicrob Agents Chemother*, 51(6), 1897-1904. doi:10.1128/AAC.01092-06
- Nandakumar, M. P., Shen, J., Raman, B., & Marten, M. R. (2003). Solubilization of trichloroacetic acid (TCA) precipitated microbial proteins via NaOH for two-dimensional electrophoresis. *J Proteome Res*, 2(1), 89-93. doi:10.1021/pr025541x
- Paul, S., Stamnes, M., Thomas, G. H., Liu, H., Hagiwara, D., Gomi, K., . . . Moye-Rowley, W. S. (2019). AtrR Is an Essential Determinant of Azole Resistance in *Aspergillus fumigatus*. *mBio*, 10(2), e02563-02518. doi:10.1128/mBio.02563-18
- Shapiro, R. S., Robbins, N., & Cowen, L. E. (2011). Regulatory circuitry governing fungal development, drug resistance, and disease. *Microbiol Mol Biol Rev*, 75(2), 213-267. doi:10.1128/MMBR.00045-10
- Snelders, E., van der Lee, H. A., Kuijpers, J., Rijs, A. J., Varga, J., Samson, R. A., . . . Verweij, P. E. (2008). Emergence of azole resistance in *Aspergillus fumigatus* and spread of a single resistance mechanism. *PLoS Med*, 5(11), e219. doi:10.1371/journal.pmed.0050219
- Song, J. X., Zhai, P. F., & Lu, L. (2017). Damage resistance protein (Dap) contributes to azole resistance in a sterol-regulatory-element-binding protein SrbA-dependent way. *Appl Microbiol Biotechnol*, 101(9), 3729-3741. doi:10.1007/s00253-016-8072-9
- Steidl, S., Hynes, M. J., & Brakhage, A. A. (2001). The *Aspergillus nidulans* multimeric CCAAT binding complex AnCF is negatively autoregulated via its *hapB* subunit gene. *J Mol Biol*, 306(4), 643-653. doi:DOI 10.1006/jmbi.2001.4412
- Traunmuller, F., Popovic, M., Konz, K. H., Smolle-Juttner, F. M., & Joukhadar, C. (2011). Efficacy and safety of current drug therapies for invasive aspergillosis. *Pharmacology*, 88(3-4), 213-224. doi:10.1159/000331860
- Vaknin, Y., Hillmann, F., Iannitti, R., Ben Baruch, N., Sandovsky-Losica, H., Shadkchan, Y., . . . Osherov, N. (2016). Identification and Characterization of a Novel *Aspergillus fumigatus* Rhomboid Family Putative Protease, RbdA, Involved in Hypoxia Sensing and Virulence. *Infect and Immun*, 84(6), 1866-1878. doi:10.1128/iai.00011-16
- Wei, X., Chen, P., Gao, R., Li, Y., Zhang, A., Liu, F., & Lu, L. (2017). Screening and Characterization of a Non-

cyp51A Mutation in an *Aspergillus fumigatus* *cox10* Strain Conferring Azole Resistance. *Antimicrob Agents Chemother*, 61(1), e02101-02116. doi:10.1128/AAC.02101-16

Willger, S. D., Cornish, E. J., Chung, D., Fleming, B. A., Lehmann, M. M., Puttikamonkul, S., & Cramer, R. A. (2012). Dsc Orthologs Are Required for Hypoxia Adaptation, Triazole Drug Responses, and Fungal Virulence in *Aspergillus fumigatus*. *Eukaryot Cell*, 11(12), 1557-1567. doi:10.1128/Ec.00252-12

Willger, S. D., Puttikamonkul, S., Kim, K. H., Burritt, J. B., Grahl, N., Metzler, L. J., . . . Cramer, R. A., Jr. (2008). A sterol-regulatory element binding protein is required for cell polarity, hypoxia adaptation, azole drug resistance, and virulence in *Aspergillus fumigatus*. *PLoS Pathog*, 4(11), e1000200. doi:10.1371/journal.ppat.1000200

Zhang, C., & Lu, L. (2017). Precise and Efficient In-Frame Integration of an Exogenous GFP Tag in *Aspergillus fumigatus* by a CRISPR System. *Methods Mol Biol*, 1625, 249-258. doi:10.1007/978-1-4939-7104-6_17

Zhang, C., Meng, X., Gu, H., Ma, Z., & Lu, L. (2018). Predicted Glycerol 3-Phosphate Dehydrogenase Homologs and the Glycerol Kinase GlcA Coordinately Adapt to Various Carbon Sources and Osmotic Stress in *Aspergillus fumigatus*. *G3 (Bethesda)*, 8(7), 2291-2299. doi:10.1534/g3.118.200253

Zhang, C., Meng, X., Wei, X., & Lu, L. (2016). Highly efficient CRISPR mutagenesis by microhomology-mediated end joining in *Aspergillus fumigatus*. *Fungal Genet Biol*, 86, 47-57. doi:10.1016/j.fgb.2015.12.007

Zhang, J. X., Li, L. P., Lv, Q. Z., Yan, L., Wang, Y., & Jiang, Y. Y. (2019). The Fungal CYP51s: Their Functions, Structures, Related Drug Resistance, and Inhibitors. *Front Microb*, 10, 691. doi:10.3389/fmicb.2019.00691

Figure Legends

Figure 1. Dysfunction of the HapB/CBC complex leads to the resistance of 415-2 isolate to azoles.

(a) A series of 2×10^4 conidia of wild-type (A1160::*pyr4/ZC03*) 415-2 isolate, 415-2^{*hapB*}, Δ *hapB/C/E*, *hapB^c*, and *hapB¹⁶⁵* strains were spotted onto MMUU (MM plus 5 mM uridine and 10 mM uracil) with different concentrations of ITC or VRC cultured at 37°C for 2 days or 4 days.

(b) The pie chart reflects the mutations in the 415-2 genome by SNPs analysis.

Figure 2. Increased expression of Erg11A and azole resistance induced by loss of HapB is dependent on *SrbA*.

(a) Western blotting using a GFP antibody showed the protein expression levels of Erg11A-GFP in the parental wild-type, Δ *hapB*, Δ *srbA*, and Δ *hapB* Δ *srbA* strains. These strains were grown in 100 ml of MM at 37°C for 24 h, and then 0.2% DMSO or 16 μ g/ml ITC was added to the media for 4 h. Immunoblot with an antibody against actin and Coomassie brilliant blue protein staining (CBB) of the total protein in SDS-PAGE gels were used as two internal loading controls.

(b) GFP signals of the fusion protein Erg11A-GFP were observed in the indicated strains grown in MM at 37°C for 12 h and then shifted into MM with DMSO or ITC for 4 h. Hoechst was used to visualize the nuclei. The scale bar is 5 μ m.

(c) A series of 2×10^4 conidia of the indicated strains were spotted onto solid MMUU with different concentrations of ITC and VRC cultured at 37°C for 2 days or 4 days.

Figure 3. The protein expression and localization of *SrbA* and HapB.

(a) and (c) The GFP-*SrbA* and GFP-HapB strains were grown in MM for 12 h and then shifted into

MM with or without 0.2% DMSO or 16 $\mu\text{g/ml}$ ITC for 2 h. The scale bar is 5 μm .

(b) and (d) The indicated strains were grown in MM at 37°C for 24 h, and then 0.2% DMSO or 16 $\mu\text{g/ml}$ ITC was added to the media for 2 h. The control “0” indicates the strains that were grown in MM for 26 h without DMSO or ITC treatment. The protein samples extracted using the alkaline lysis strategy or nucleoprotein extraction kit were examined by immunoblotting. The wild-types strain without GFP tag was used as a control.

Figure 4. The nuclear form of SrbA renders *A. fumigatus* resistant to azole and increases the expression of Erg11A.

(a) Prediction of a basic helix-loop-helix (bHLH) motif, transmembrane (TM), and DUF2014 domain in SrbA based on a SMART protein search (<http://smart.embl-heidelberg.de/>) was performed, and a schematic is shown for the design of GFP-SrbA and GFP-SrbA^T constructs for detection of SrbA localization.

(b) Colocalization analysis of GFP-SrbA/GFP-SrbA^T and RFP-H2A was performed. The bar is 5 μm .

(c) A series of 2×10^4 conidia of SrbA^F and SrbA^T strains were spotted onto MM for 2.5 days and onto MM with ITC for 4 days.

(d) Western blotting shows the protein expression of Erg11A in the SrbA^F and SrbA^T strains.

(e) Fluorescence microscopy shows the GFP signals of Erg11A-GFP in the SrbA^F and SrbA^T strains.

Figure 5. Lack of HapB prolongs nuclear retention of SrbA and increases the protein levels of the nuclear form of SrbA.

(a) The WT^{GFP-SrbA} and $\Delta hapB$ ^{GFP-SrbA} strains were grown in MM for 12 h and then shifted into MM with 16 $\mu\text{g/ml}$ ITC for 2, 4, and 6 h. The GFP signals were observed using a fluorescence microscope. The scale bar is 5 μm .

(b) The indicated strains were grown in MM at 37°C for 24 h, and then 16 µg/ml ITC was added to the media for 4 h. The protein samples extracted by the nucleoprotein extraction kit were examined by immunoblotting.

(c) The transcript levels of *srbA* in the wild-type and $\Delta hapB$ strains grown in MM for 16 h and 24 h. Statistical significance was determined by Student's *t*-test. ** $p < 0.01$. Values are means \pm SD from three independent replicates.

(d) EMSA analysis of CBC binding to Cy5-labeled promoter fragments of *srbA*. Two specific probes (1 and 2,) were designed for *srbA*. *srbA* probe 1/2 contains the CCAAT motif located at position 986/195 bp (-986/-195) upstream of the *srbA* translational start site. The specificity of EMSA binding was validated by using a mutant probe or adding specific competitors/cold probe (unlabeled probe).

Figure 6. HapB regulates the expression of the proteins associated with the proteolytic cleavage of SrbA.

(a) The putative schematic diagram of cleavage of *A. fumigatus* SrbA.

(b) qRT-PCR showed the mRNA expression of *dscA-E*, *rbdB*, *sppA* in the wild-type and $\Delta hapB$ backgrounds. The indicated strains were grown in MM at 37°C for 16 h, 20 h, and 24 h. Statistical significance was determined by Student's *t*-test. * $p < 0.05$; ** $p < 0.01$; ns, not significant. Values are means \pm SD from three independent replicates.

(c) EMSA analysis of CBC binding to Cy5-labeled promoter fragments of *dscE*, *rbdB*, and *sppA*. Probes of *dscE/rbdB/sppA* contain the CCAAT motif located at -1467/-600/-170 position of their promoters, respectively.

(d) Western blotting the protein of DscC-E and SppA in the wild-type and $\Delta hapB$ backgrounds. The indicated strains were grown in MM at 37°C for 24 h.

Figure 7. A proposed model is shown highlighting the mechanistic basis of *erg11A* expression regulated by CBC and SrbA.

By directly interacting with the 34 *mer* region of the *erg11A* promoter, CBC and SrbA negatively and positively regulate the expression of *erg11A*, respectively. Upon azole stress, full-length SrbA (SrbA-F) is cleaved into the nuclear form (SrbA-N) and subsequently transfers from the endoplasmic reticulum (ER) into the nucleus to exert its function. CBC not only represses the expression of *srbA* but also inhibits SrbA cleavage and nuclear translocation via repressing the expression of SrbA cleavage-associated genes, including *rbdB*, Dsc complex genes, and *sppA*. These repressions are liberated in the mutants of CBC. Notably, CBC dysfunction also prolongs the retention time of SrbA-N in the nucleus, which is not represented in the model.

Appendix

Table A1. Strains used in this study.

Strains	Genotype	Source
ZC03/WT	$\Delta ku80$; <i>pyrG1</i> ; <i>AMA1::P_{gpdA}::Cas9::pyr4</i> ;	From Lu Lab
415-2	$\Delta ku80$; <i>pyrG1</i> ; $\Delta algA::pyr4$; <i>hapB^{Q166}</i>	From Lu Lab
415-2 ^{hapB}	$\Delta ku80$; <i>pyrG1</i> ; $\Delta algA::pyr4$; <i>hapB^{Q165}</i> ; <i>hapB::hph</i>	This study
$\Delta hapB$	ZC03; $\Delta hapB::hph$	From Lu Lab
<i>hapB^c</i>	$\Delta ku80$; <i>pyrG1</i> ; $\Delta hapB::hph$; <i>hapB::pyr4</i>	From Lu Lab
<i>hapB¹⁶⁵</i>	ZC03; <i>hapB^{Q165}::hph</i>	This study
$\Delta hapC$	ZC03; $\Delta hapC::hph$	From Lu Lab
$\Delta hapE$	ZC03; $\Delta hapE::hph$	From Lu Lab
Erg11A-GFP	ZC03; <i>erg11A-gfp::ptrA</i>	This study
$\Delta hapB^{\text{Erg11A-GFP}}$	ZC03; $\Delta hapB::hph$; <i>erg11A-gfp::ptrA</i>	This study
$\Delta srbA^{\text{Erg11A-GFP}}$	$\Delta ku80$; <i>pyrG1</i> ; $\Delta srbA::pyr4$; <i>erg11A-gfp::ptrA</i>	This study
$\Delta hapB\Delta srbA^{\text{Erg11A-GFP}}$	$\Delta ku80$; <i>pyrG1</i> ; $\Delta srbA::pyr4$; $\Delta hapB::hph$; <i>erg11A-gfp::ptrA</i>	This study
$\Delta hapB\Delta erg11A$	ZC03; $\Delta hapB::hph$; $\Delta erg11A::ptrA$	This study
$\Delta erg11A$	ZC03; $\Delta erg11A::ptrA$	This study
$\Delta srbA$	$\Delta ku80$; <i>pyrG1</i> ; $\Delta srbA::pyr4$	This study
$\Delta hapB\Delta srbA$	$\Delta ku80$; <i>pyrG1</i> ; $\Delta srbA::pyr4$; <i>hapB::hph</i>	This study
WT ^{GFP-SrbA}	$\Delta ku80$; <i>pyrG1</i> ; <i>AMA1::P_{srbA}::gfp::srbA::pyr4</i>	This study
GFP-HapB	ZC03; <i>gfp::hapB</i> ; <i>hph</i>	From Lu Lab
GFP-SrbA ^{RFP-H2A}	$\Delta ku80$; <i>pyrG1</i> ; <i>AMA1::P_{srbA}::gfp::srbA::P_{gpdA}::rfp::H2A::pyr4</i>	This study
GFP-SrbA ^T RFP-H2A	$\Delta ku80$; <i>pyrG1</i> ; <i>AMA1::P_{srbA}::gfp::srbA¹⁻³⁸⁰::P_{gpdA}::rfp::H2A::pyr4</i>	This study
SrbA ^F	$\Delta ku80$; <i>pyrG1</i> ; <i>AMA1::P_{srbA}::srbA::pyr4</i>	This study
SrbA ^T	$\Delta ku80$; <i>pyrG1</i> ; <i>AMA1::P_{srbA}::srbA¹⁻³⁸⁰::pyr4</i>	This study
SrbA ^T Erg11A-GFP	$\Delta ku80$; <i>pyrG1</i> ; <i>erg11A-gfp::ptrA</i> ; <i>AMA1::P_{srbA}::srbA¹⁻³⁸⁰::pyr4</i>	This study
$\Delta hapB^{\text{GFP-SrbA}}$	$\Delta ku80$; <i>pyrG1</i> ; $\Delta hapB::hph$; <i>AMA1::P_{srbA}::gfp::srbA::pyr4</i>	This study
SppA-GFP	ZC03; <i>sppA-gfp::ptrA</i>	This study
$\Delta hapB^{\text{SppA-GFP}}$	ZC03; $\Delta hapB::hph$; <i>sppA-gfp::ptrA</i>	This study
DscA-GFP	ZC03; <i>dscA-gfp::ptrA</i>	This study
$\Delta hapB^{\text{DscA-GFP}}$	ZC03; $\Delta hapB::hph$; <i>dscA-gfp::ptrA</i>	This study
DscB-GFP	ZC03; <i>dscB-gfp::ptrA</i>	This study
$\Delta hapB^{\text{DscB-GFP}}$	ZC03; $\Delta hapB::hph$; <i>dscB-gfp::ptrA</i>	This study
DscC-GFP	ZC03; <i>dscC-gfp::ptrA</i>	This study
$\Delta hapB^{\text{DscC-GFP}}$	ZC03; $\Delta hapB::hph$; <i>dscC-gfp::ptrA</i>	This study
DscD-GFP	ZC03; <i>dscD-gfp::ptrA</i>	This study
$\Delta hapB^{\text{DscD-GFP}}$	ZC03; $\Delta hapB::hph$; <i>dscD-gfp::ptrA</i>	This study
DscE-GFP	ZC03; <i>dscE-gfp::ptrA</i>	This study
$\Delta hapB^{\text{DscE-GFP}}$	ZC03; $\Delta hapB::hph$; <i>dscE-gfp::ptrA</i>	This study
RbdB-GFP	ZC03; <i>rbdB-gfp::ptrA</i>	This study
$\Delta hapB^{\text{RbdB-GFP}}$	ZC03; $\Delta hapB::hph$; <i>rbdB-gfp::ptrA</i>	This study

Table A2. Primers used in this study.

Name	Sequence	Intention
sgRNA-R	AAAAAAGCACCGACTCGGTGCC	for the DNA template of sgRNA
T7-hapB-sgRNA2-F	TAATACGACTCACTATAGGGATAGTTGGGTGCCATT GTTTTAGAGCTAGAAATAGC	for the DNA template of hapB-sgRNA2 (RNA); for constructing <i>hapB</i> ¹⁶⁵
hapB ^T -hph-R	CTCATACGACGCTGTTGCATCTGGGCATTTTGGGTC GAGTGGAGATGTGGAGTGGG	for the repair template of <i>hapB</i> truncation
hapB ^T -hph-F	AGATTTTCAGGACAGATG CCC ATG GGT ACA TAA	for the repair template of <i>hapB</i> truncation
hapB-seq-F	ACTCGAGCTGTTACTGGGTTAAG	diagnostic primer for <i>hapB</i> ¹⁶⁵
hapB-seq-R	ATGAGCCGATCGACAAGAGGGTA	diagnostic primer for <i>hapB</i> ¹⁶⁵
SrbAP1	AAATGGGTTTCGTTGTATG	for deleting <i>srbA</i>
SrbAP2	TCTCCAGGTTGATATTGTTC	for deleting <i>srbA</i>
SrbAP3	CGATTAAGTTGGGTAACGCCACTTGACGGTGGAGTT AGA	for deleting <i>srbA</i>
SrbAP4	ATAAGTAGCCAGTTCCCGAAAGCACCAAGATGTGCC TCCAA	for deleting <i>srbA</i>
SrbAP5	GATGATGTCCGGTAGGTGC	for deleting <i>srbA</i>
SrbAP6	GATCCCTCCATTCACCAG	for deleting <i>srbA</i>
Pyr4-F	TGGCGTTACCCAACCTTAATCG	for amplifying <i>pyr4</i>
Pyr-R	GCTTTCGGGAAGTGGCTACTTAT	for amplifying <i>pyr4</i>
SrbA-F	AAACTCAACAAAGCGTCCAT	diagnostic primer for Δ <i>srbA</i>
SrbA-R	CTGCGGGCAACATCATTG	diagnostic primer for Δ <i>srbA</i>
T7-erg11A-sgRNA-F	TAATACGACTCACTATAGGGATTTGGTGTGATCGGAA TGTTTTAGAGCTAGAAATAGC	for the DNA template of erg11A-sgRNA (RNA); for deleting and tagging <i>erg11A</i>
erg11-deletionptrA-F	TCTAATCCTCGGGCTCACCCCTCCCTGTGTCTCCTCG AAGCCTAGATGGCCTCTTGCATC	for the repair template of deleting and tagging <i>erg11A</i>
erg11-deletionptrA-R	CTCGAGGGGCTGAATTAAGTATAATACACCTATTTCAT GGCAGACACTGAAGCAAC	for the repair template of deleting <i>erg11A</i>
gfp-erg11A-F	CGGCTGGGAGAAGCGGTCGAAAAACACATCCAAGG GAGCTGGTGCAGGCGCTGG	for the repair template of tagging <i>erg11A</i>
erg11A-seq-F	CATTTCCCTCATCACTGCAACTC	diagnostic primer for Δ <i>erg11A</i> and <i>erg11A-gfp</i>
erg11A-seq-R	GTATAGGCAACAACACTTCAGGG	diagnostic primer for Δ <i>erg11A</i> and <i>erg11A-gfp</i>
Ama1-srbA-F	CGGTTATGCCGTATGGATCCGATAGACTTCAGGTTA GTGATAGG	for amplifying P _{srbA} -gfp-srbA fragment

Ama1-srbA-R	AATCAGCCTAGCTAGGATCCCTACGACTCATCGGAGAGC	for amplifying P_{srbA} -gfp-srbA fragment
gpd-srbA-R	CGTCCGTCTCTCCGCATGCCTACGACTCATCGGAGAGC	for amplifying P_{srbA} -gfp-srbA fragment (coupled with Ama1-srbA-F)
gpd-F	GCATGCGGAGAGACGGACG	for amplifying P_{gpdA} -rfp-H2A fragment
Ama1-trpC-R	AATCAGCCTAGCTAGGATCCCATGCATTGCAGATGAGCTG	for amplifying P_{gpdA} -rfp-H2A fragment
Ama1-srbA ^T -R	AATCAGCCTAGCTAGGATCCCTATTCTGTGCCTAGGCCTTCAAG	for amplifying P_{srbA} -gfp-srbA ^T / P_{srbA} -srbA ^T fragment, coupled with Ama1-srbA-F
gpd-srbA ^T -R	CGTCCGTCTCTCCGCATGCCTATTCTGTGCCTAGGCCTTCAAG	for amplifying P_{srbA} -gfp-srbA ^T fragment (coupled with Ama1-srbA-F)
T7-sppA-sgRNA-F	TAATACGACTCACTATAGGGAGTTCTTTCTTTCTGTGTTTTAGAGCTAGAAATAGC	for the DNA template of sppA-sgRNA (RNA); for tagging <i>sppA</i>
sppA-gfp-F	CAAGGCCAGCTTGTGGGTACATTGTCGGAAGGAGCTGGTGCAGGCGCTG	for the repair template of tagging <i>sppA</i>
sppA-ptrA-R	GTTCTCCTCTGAGGAGCGCAGTCCCCACACTAGGAGATCGTCCGCCGATG	for the repair template of tagging <i>sppA</i>
sppA-seq-F	CCGTTAATGGTGACAGTCGCT	diagnostic primer for SppA-GFP; qRT-PCR primer
sppA-seq-R	GCACCTTGTGATTTGTCATCTG	diagnostic primer for SppA-GFP
sppA-RT-R	GGAAAGGAAGATCAAATCGGAG	qRT-PCR primer
T7-dscA-sgRNA-F	TAATACGACTCACTATAGGGATGTTGTACGGACTGATGTTTTAGAGCTAGAAATAGC	for the DNA template of dscA-sgRNA (RNA); for tagging <i>dscA</i>
dscA-gfp-F	CCCATTTGTCGGGAGTCAATCCCTCCTGTAGGAGCTGGTGCAGGCGCTG	for the repair template of tagging <i>dscA</i>
dscA-ptrA-R	TTTGTGTCCTGGGATGTTGTACGGACTGATCTAGGAGATCGTCCGCCGATG	for the repair template of tagging <i>dscA</i>
dscA-seq-F	GGTACGTGGCAACGTGCTG	diagnostic primer for DscA-gfp; qRT-PCR primer
dscA-seq-R	TCGCCAAGATCGAGGTCAGTG	diagnostic primer for DscA-GFP
dscA-RT-R	CAGACTCCAGATCTGCCTCAGAC	qRT-PCR primer
dscB-RT-F	CGGTATAGGATCAGCACCAGC	diagnostic primer for DscB-gfp; qRT-PCR primer
dscB-RT-R	AACTGCGACAGAGCCAGCTG	qRT-PCR primer
T7-dscC-sgRNA-F	TAATACGACTCACTATAGGGTGCCTTCCTTCAGCCATAGTTTTAGAGCTAGAAATAGC	for the DNA template of dscC-sgRNA (RNA); for tagging <i>dscC</i>

dscC-gfp-F	GTTGCATTTGGCGCTATGCGCATTATGAATGGAGCT GGTGCAGGCGCTG	for the repair template of tagging <i>dscC</i>
dscC-ptrA-R	CTGGTCGCTTGGTGCCTTCCTTCAGCCATACTAGGA GATCGTCCGCCGATG	for the repair template of tagging <i>dscC</i>
dscC-seq-F	CGAAGACCGGTGGATGGATG	diagnostic primer for DscC-GFP; qRT-PCR primer
dscC-seq-R	CAGAGTGAAGGATATGTAGAC	diagnostic primer for DscC-GFP
dscC-RT-R	CCTCAACCACATGGCACAGC	qRT-PCR primer
T7-dscD- sgRNA-F	TAATACGACTCACTATAGGGATCTCTTCATGCCAGTG TTTTAGAGCTAGAAATAGC	for the DNA template of <i>dscD</i> -sgRNA (RNA); for tagging <i>dscD</i>
dscD-gfp-F	GTCGGGCCTGACGGTCGTGTTTCAGCGGATACAATCC GGAGCTGGTGCAGGCGCTG	for the repair template of tagging <i>dscD</i>
dscD-ptrA-R	CCAACGGTGGATAGGATCTCTTCATGCCCTAGGAGA TCGTCCGCCGATG	for the repair template of tagging <i>dscD</i>
dscD-seq-F	TGCCGGTGTAGGTGAACAGG	diagnostic primer for <i>dscD</i> - <i>gfp</i> ; qRT-PCR primer
dscD-seq-R	GATGGTGCTGGTGAAGCTTC	diagnostic primer for DscD-GFP
dscD-RT-R	CCGTCTGGTCCGAAGGTATG	qRT-PCR primer
T7-dscE- sgRNA-F	TAATACGACTCACTATAG GGTGTTGATAATGACATTAGTTTTAGAGCTAGAAATA GC	for the DNA template of <i>dscE</i> -sgRNA (RNA); for tagging <i>dscE</i>
dscE-gfp-F	GACAGCGATGAGGAAGAGCAGGAAGTATCCGGAGC TGGTGCAGGCGCTG	for the repair template of tagging <i>dscE</i>
dscE-ptrA-R	TCGCCGGGGCAGTGCGCCTGTCTACCATAACTAGGA GATCGTCCGCCGATG	for the repair template of tagging <i>dscE</i>
dscE-seq-F	ACGACATTGCGCAATGGAAG	diagnostic primer for DscE- GFP; qRT-PCR primer
dscE-yz-R	CAGTCGGTACAGACGATCGAG	diagnostic primer for DscE- GFP
dscE-RT-R	GCCCTGTGCAGCTTGCAGAAC	qRT-PCR primer
srbA-RT-F	CCAGTCAGGACTGGACACAG	qRT-PCR primer
srbA-RT-R	GGTGAGAAGTCTTTGTGCATCG	qRT-PCR primer
tubA-RT-F	TGACTGCCTCCAGGGCTTCC	qRT-PCR primer
tubA-RT-R	GCGTTGTAAGGCTCAACGAC	qRT-PCR primer
rbdB-RT-F	CTACTGCTGGGCTCTGAAGC	qRT-PCR primer, diagnostic primer for RbdB-GFP
rbdB-RT-R	CGAGACCGAGAAGATAGCCT	qRT-PCR primer
T7-rbdB-F	TAATACGACTCACTATAGGGAGGTAGGTTCAAGGAC CGGTTTTAGAGCTAGAAATAGCA	for the DNA template of <i>rbdB</i> -sgRNA (RNA); for RbdB-GFP

rbdB-gfp-F	CTATCTGGGTACGAATCAGCGCCTCGGTCCTGGAGC TGGTGCAGGCGCTGG	for the repair template of tagging <i>rbdB</i> (RbdB-GFP)
rbdB-ptrA-R	CATCGGCGGACGATCTCCTAGACCTACCTCGCTCAG CAGGGAGAGATG	for the repair template of tagging <i>rbdB</i> (RbdB-GFP)
rbdB-seq-R	CCATGCCTAGTGTGGTAGTG	diagnostic primer for RbdB-GFP
Pet30A-F	GAATTCGAGCTCCGTCGACACCAGCTTGCGGCCGCA CTCGAG	Linearization of Pet30A
Pet30A-R	CATATGTATATCTCCTTCTTAAAGTTAAAC	Linearization of Pet30A
EmsA-hapB-F	GAAGGAGATATACATATGATGGAATACCCTCCACAAT ATCAAC	Amplification of <i>hapB</i> cDNA
EmsA-hapB-R	GTCGACGGAGCTCGAATTCACCATCTTCATCGGTTG GTTC	Amplification of <i>hapB</i> cDNA
EmsA-hapC-F	GAAGGAGATATACATATGATGTGCGCCTCTCCCTCG AAAG	Amplification of <i>hapC</i> cDNA
EmsA-hapC-R	GTCGACGGAGCTCGAATTCGTACGAGTCGCCTCCTG CTC	Amplification of <i>hapC</i> cDNA
EmsA-hapE-F	GAAGGAGATATACATATGATGGAACAGTCTTCGCAG AGCAC	Amplification of <i>hapE</i> cDNA
EmsA-hapE-R	GTCGACGGAGCTCGAATTCAGAAGAGTTTTGGCATA CCTGC	Amplification of <i>hapE</i> cDNA
EmsA-srbA2-F	AGATGCAGCTAGCACGCCAGGTTGATATTGTTCCAAT GGTGTCTCAGATACAGATACTTC	for <i>srbA</i> probe 2
EmsA-srbA2-MF	AGATGCAGCTAGCACGCCAGGTTGATATTGTTTCAGA TGGTGTCTCAGATACAGATACTTC	for <i>srbA</i> mutant probe 2
EmsA-srbA2-R	AGATGCAGCTAGCACGCTGTCTGAAGCCGTTTCATCT	for <i>srbA</i> probe 2, for <i>srbA</i> mutant probe 2
EmsA-srbA1-F	AGATGCAGCTAGCACGCTGATTAGCGTGCTCGAATT GGGCGATCATCAATCATCGT	for <i>srbA</i> probe 1
EmsA-srbA1-MF	AGATGCAGCTAGCACGCTGATTAGCGTGCTCGAACT AGGCGATCATCAATCATCGT	for <i>srbA</i> mutant probe 1
EmsA-srbA1-R	AGATGCAGCTAGCACGACCTGTCAAGACCTGAGACG	for <i>srbA</i> probe 1, for <i>srbA</i> mutant probe 1
EmsA-sppA-F	AGATGCAGCTAGCACGCTTGTCTTGGCATCTATCATT GGGAAACACAGGGCTTTGAC	for <i>sppA</i> probe
EmsA-sppA-MF	AGATGCAGCTAGCACGCTTGTCTTGGCATCTATCATC TGGAAACACAGGGCTTTGAC	for <i>sppA</i> mutant probe
EmsA-sppA-R	AGATGCAGCTAGCACGGTTGCTCTGTGGTTGGAAAT C	for <i>sppA</i> probe, for <i>sppA</i> mutant probe
EmsA-1467-dscE-F	AGATGCAGCTAGCACGGCCAGGAGTGCTGGCATTG GATCCTTCTCACTATTAGCAG	for <i>dscE</i> probe targeting -1467 region
EmsA-1467-dscE-MF	AGATGCAGCTAGCACGGCCAGGAGTGCTGGCATCT GATCCTTCTCACTATTAGCAG	for <i>dscE</i> mutant probe targeting -1467 region
EmsA-1467-dscE-R	AGATGCAGCTAGCACGCAAAGCTGCAAATGCAGCT CC	for <i>dscE</i> probe and <i>dscE</i> mutant probe targeting -1467 region
EmsA-862-dscE-F	AGATGCAGCTAGCACGCATCCACGAGGCTCCCAATG TACGAGACCCTCTGTTCAG	for <i>dscE</i> probe targeting -862 region

EmsA-862-dscE-MF	AGATGCAGCTAGCACGCATCCACGAGGCTCCTAGTG TACGAGACCCTCTGTTCAG	for <i>dscE</i> mutant probe targeting -862 region
EmsA-862-dscE-R	AGATGCAGCTAGCACGAAGCCTGCTTTGGACGATTC	for <i>dscE</i> probe and <i>dscE</i> mutant probe targeting -862 region
EmsA-728-dscE-F	AGATGCAGCTAGCACGCTCAAGCCAAACTGACCTC	for <i>dscE</i> probe and <i>dscE</i> mutant probe targeting -728 region
EmsA-728-dscE-R	AGATGCAGCTAGCACGCGCTGATCCCCGCCAAATTG GATAAAGACATACCATGGCTTC	for <i>dscE</i> probe targeting -728 region
EmsA-728-dscE-MR	AGATGCAGCTAGCACGCGCTGATCCCCGCCAAATCT GATAAAGACATACCATGGCTTC	for <i>dscE</i> mutant probe targeting -728 region
EmsA-600-RbdB-F	AGATGCAGCTAGCACGATATATCTCATATATAATTGG TCATGATTTAATGAGCTAGAAG	for <i>rbdB</i> probe targeting -600 region
EmsA-600-RbdB-MF	AGATGCAGCTAGCACGATATATCTCATATATAAGCTG TCATGATTTAATGAGCTAGAAG	for <i>rbdB</i> mutant probe targeting -600 region
EmsA-600-RbdB-R	AGATGCAGCTAGCACGTGGGCTCTTCCAGTAACGCG	for <i>rbdB</i> probe and <i>rbdB</i> mutant probe targeting -600 region
EmsA-300-RbdB-F	AGATGCAGCTAGCACGCTTCTGCATTGTTTGTATCCA ATCTAGACAGTGACACTGCAC	for <i>rbdB</i> probe targeting -300 region
EmsA-300-RbdB-MF	AGATGCAGCTAGCACGCTTCTGCATTGTTTGTATATG ATCTAGACAGTGACACTGCAC	for <i>rbdB</i> mutant probe targeting -300 region
EmsA-300-RbdB-R	AGATGCAGCTAGCACGCGTGGTTTAATAATCAGTCAA G	for <i>rbdB</i> probe and <i>rbdB</i> mutant probe targeting -300 region

Appendix Figures

Figure A1. The growth phenotype of GFP-tagged *SrbA*/*HapB* strains on MM with or without ITC stress.

A series of 2×10^4 conidia of wild-type, $WT^{GFP-SrbA}$, GFP-*HapB* and $\Delta hapB$ and $\Delta hapB^{GFP-SrbA}$ strains were spotted onto MM with or without ITC and cultured at 37°C for 2 days or 4 days.

Figure A2. The relative *srbA* copy number in the related strains constructed by using the AMA1 vector.

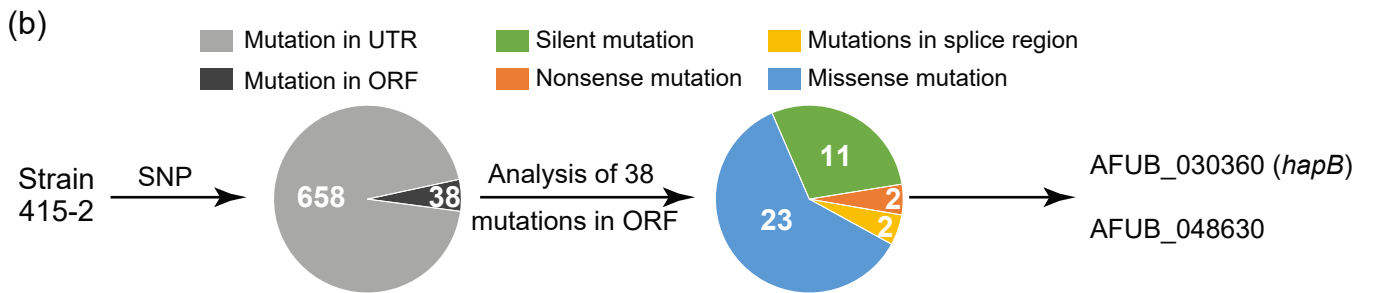
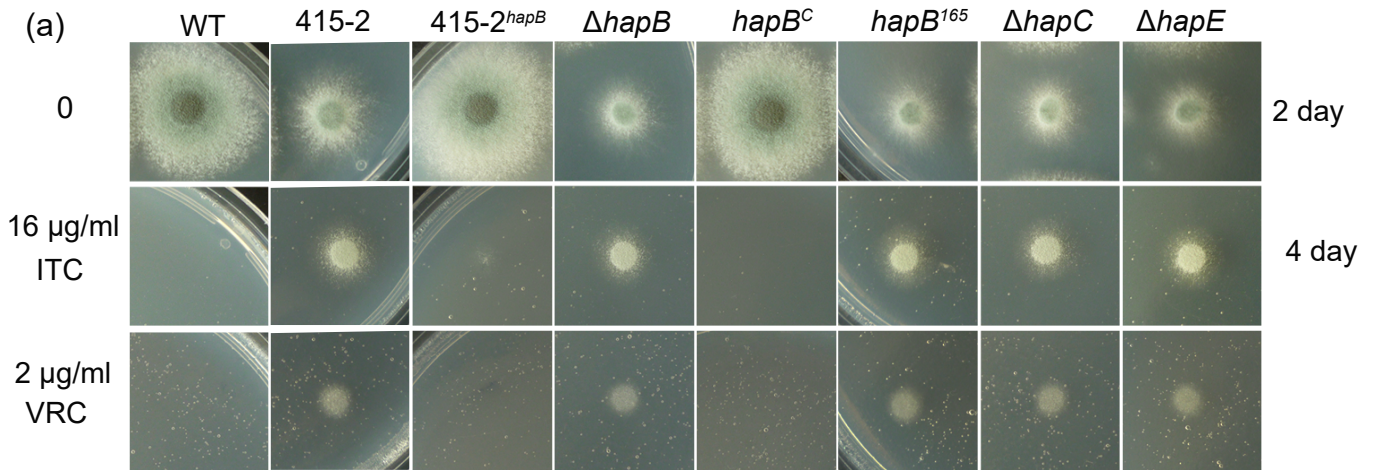
The related strains were grown in liquid MM with 220 rpm shaking at 37°C for 24 h. The respective genome was extracted from the resulting mycelium. Then qRT-PCR was used to detect the relative *srbA* copy number, *tubA* gene was used as an endogenous control. Statistical significance was determined by Student's *t*-test. ns, not significant. Values are means \pm SD from three independent replicates.

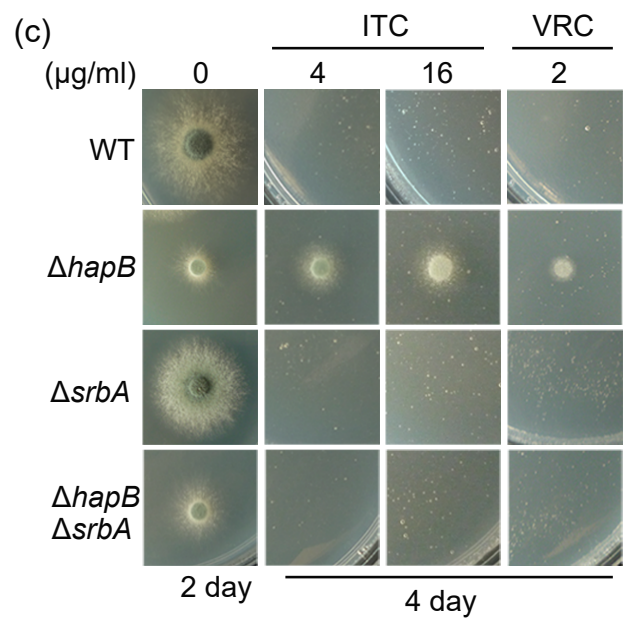
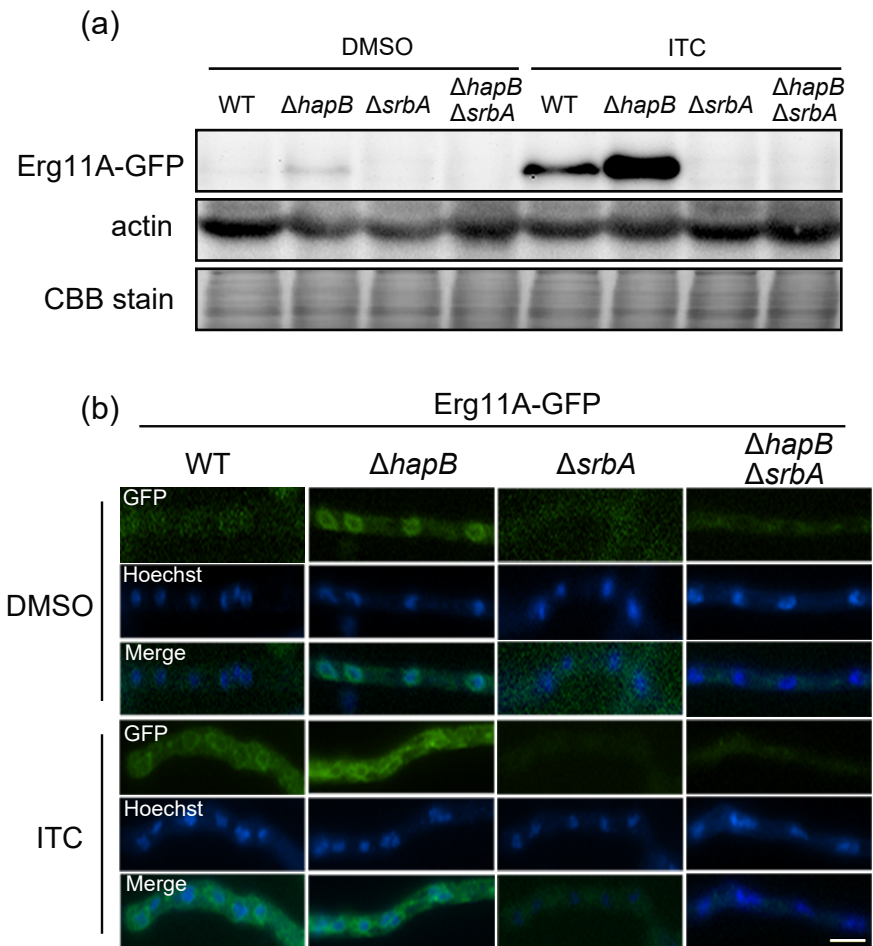
Figure A3. EMSA analysis of CBC binding to Cy5-labeled promoter fragments of *dscE* and *rbdB*.

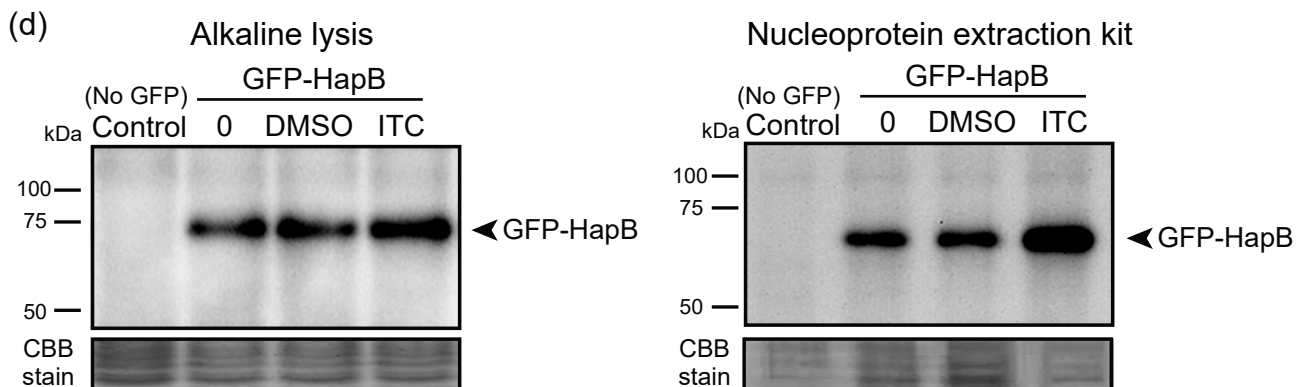
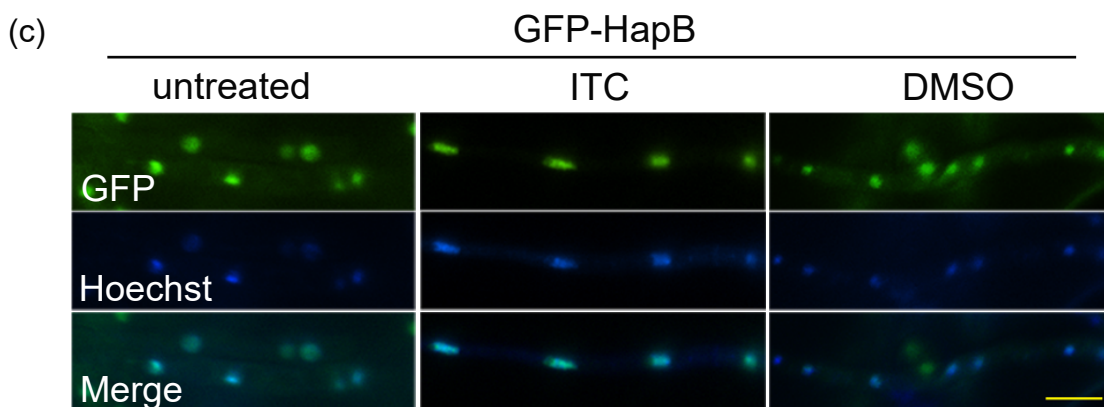
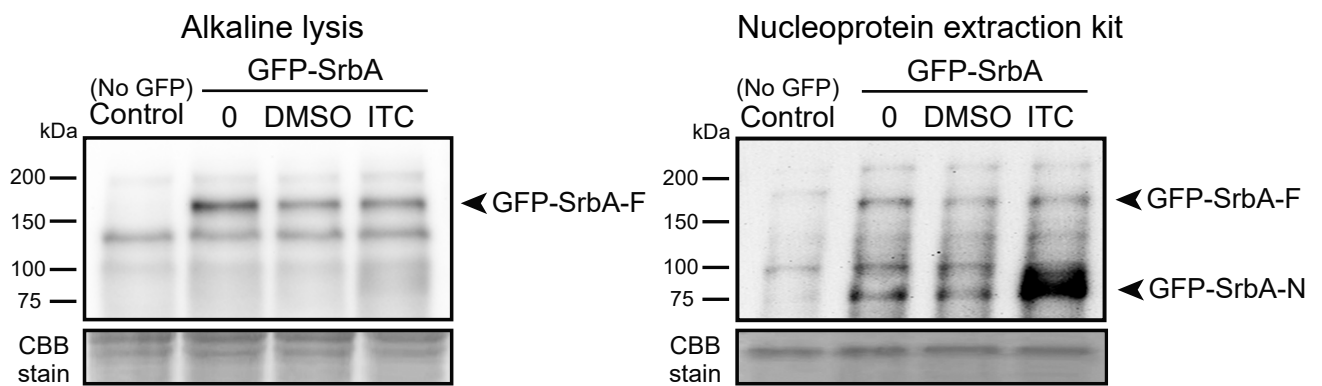
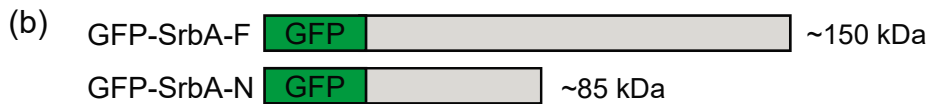
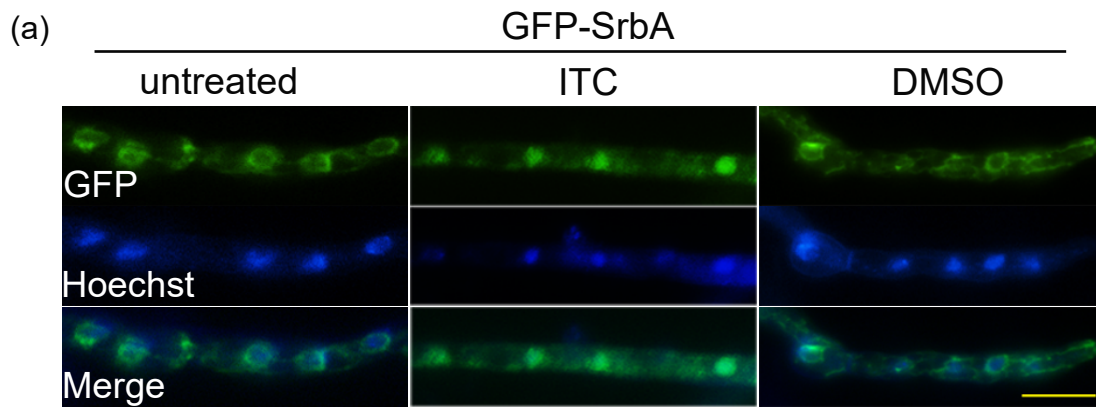
The probe of *dscE* contains a CCAAT motif located at the -862/-728 position of its promoter. The probe of *rbdB* contains a CCAAT motif located at the -300 position of its promoter.

Figure A4. The growth phenotype of the GFP-tagged *SppA*, *DscA*, *DscC-E*, and *RbdB* strains on MM.

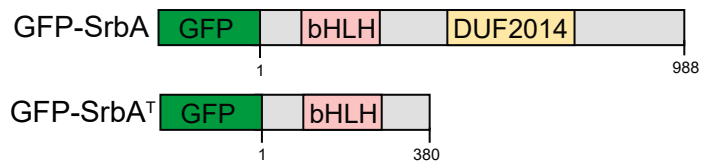
A series of 2×10^4 conidia of related strains were spotted onto MM and cultured at 37°C for 2 days.



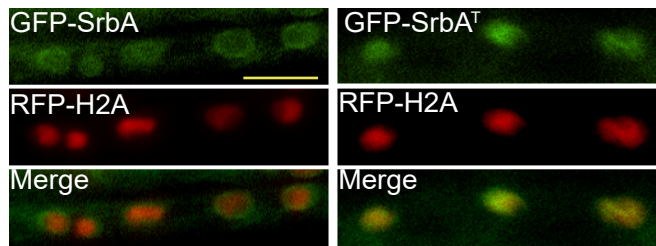




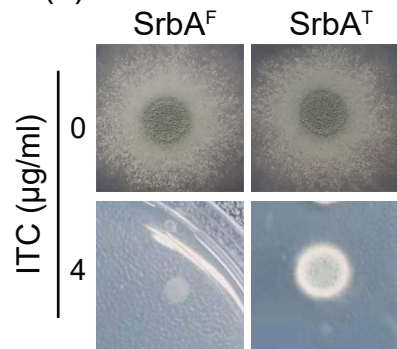
(a)



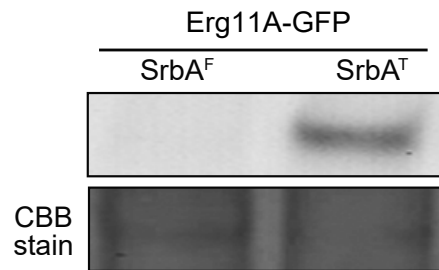
(b)



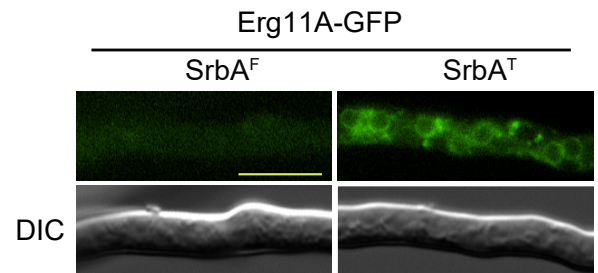
(c)

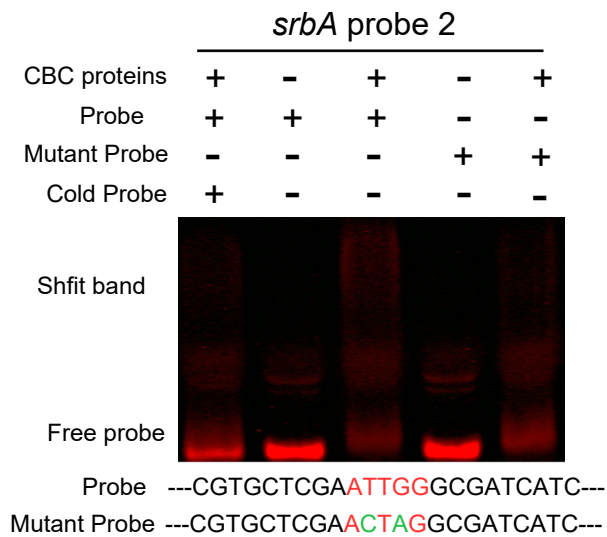
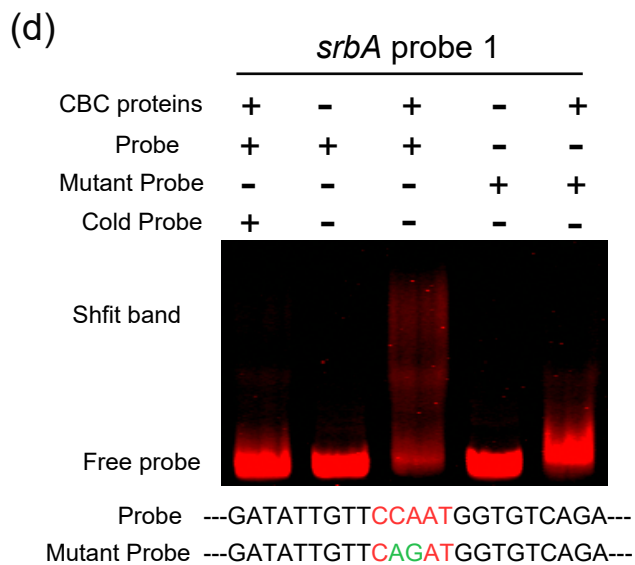
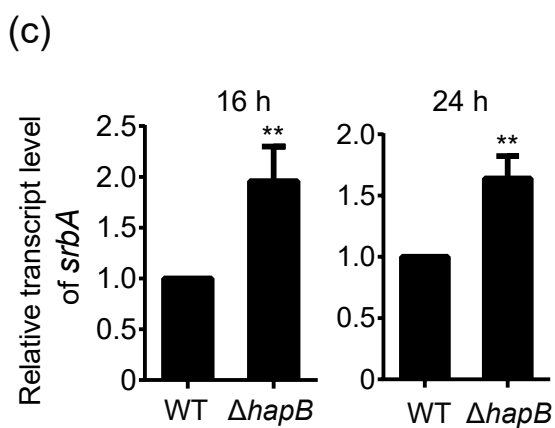
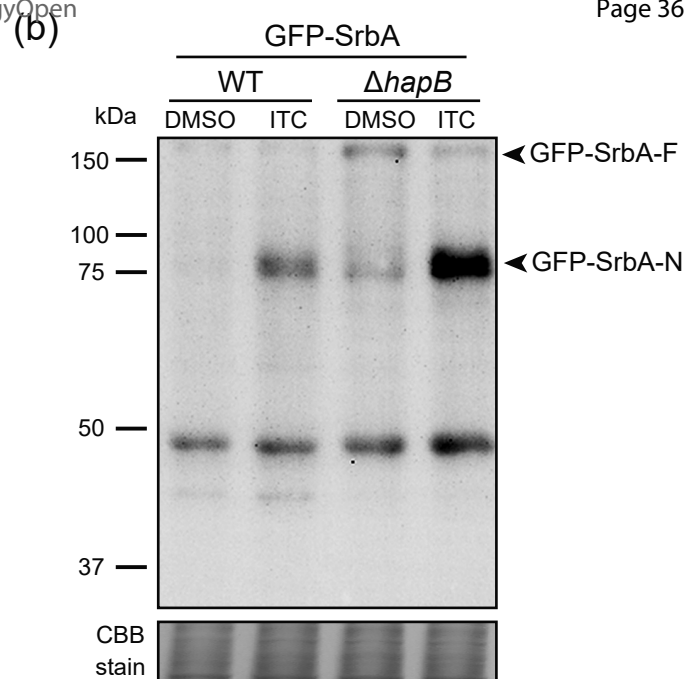
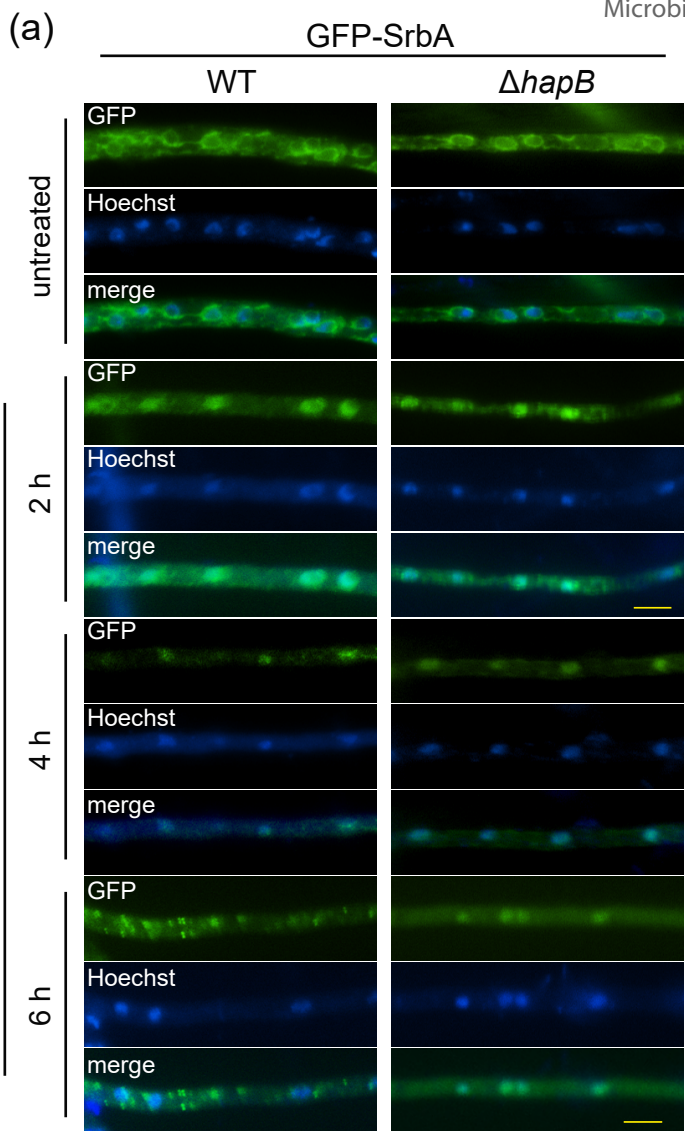


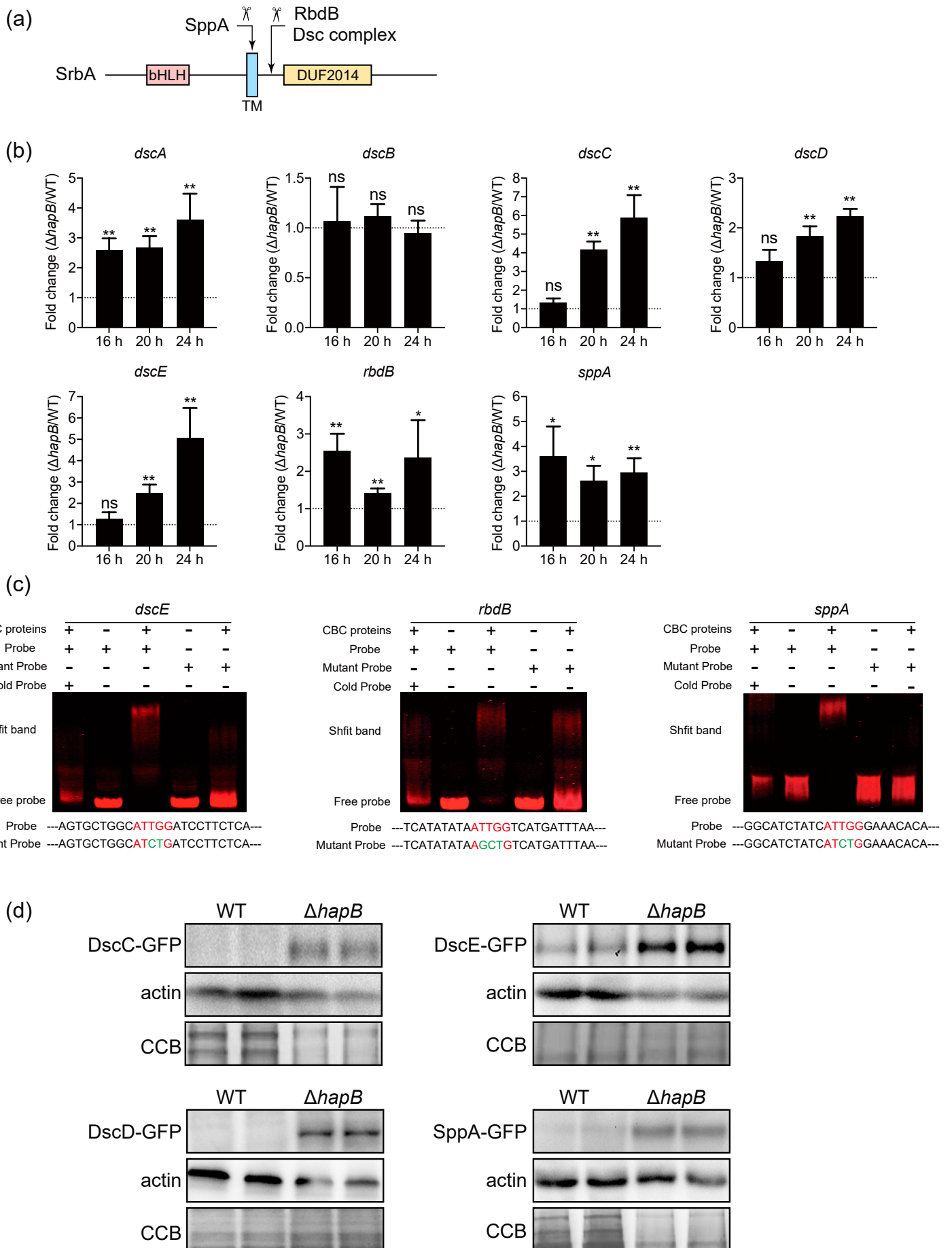
(d)



(e)







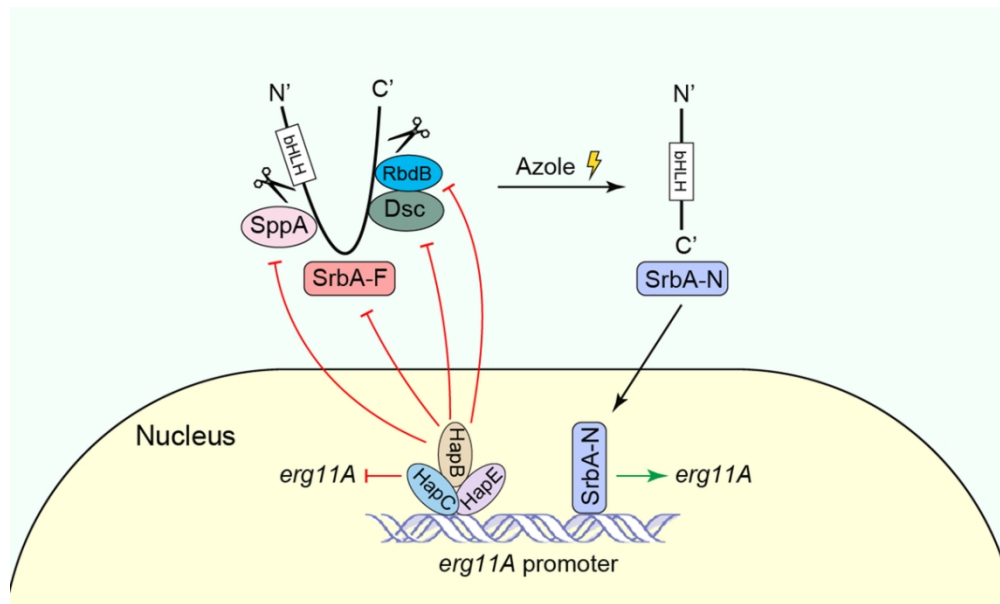


Figure 7

102x61mm (300 x 300 DPI)

